

# We are IntechOpen, the world's leading publisher of Open Access books Built by scientists, for scientists

5,300

Open access books available

130,000

International authors and editors

155M

Downloads

Our authors are among the

154

Countries delivered to

TOP 1%

most cited scientists

12.2%

Contributors from top 500 universities



WEB OF SCIENCE™

Selection of our books indexed in the Book Citation Index  
in Web of Science™ Core Collection (BKCI)

Interested in publishing with us?  
Contact [book.department@intechopen.com](mailto:book.department@intechopen.com)

Numbers displayed above are based on latest data collected.  
For more information visit [www.intechopen.com](http://www.intechopen.com)



# Passive and Active Topologies Investigation for LED Driver Circuits

*Salvatore Musumeci*

## Abstract

In this chapter, a survey of LED driver circuits is presented. The driver circuit is a crucial component in the LED light system. It provides the correct voltage and current values for the best brightness and long life. Furthermore, the driver circuits contribute to obtaining high efficiency and reliability light system. Several lighting applications need different driver topologies that meet the use requirement and the energy sources available. In actual applications, passive and active circuits are implemented to satisfy the LED driver electrical requirements and cost-effective demands. The LED driver circuits investigation evaluate the issues and the solutions in the LED lighting systems connected to a DC source such as a battery or AC line. The AC line connection requisites such as the power factor correction and the harmonic distortion are dealt with both the driver topology and control optimization. Also, the volume reduction need is examined in the circuitry choice. Moreover, the different topologies of the power converters isolated and not isolated used in the driver circuits based on both the power request and supply source are described and critically evaluated.

**Keywords:** LED driver, linear driver circuits, DC-DC converter, Flyback, PFC, LLC converter, multi-channel LED, average current control, peak current control

## 1. Introduction

Nowadays, LED lights are becoming more and more used in various fields of applications such as domestic and industrial lighting, open space offices or supermarkets lighting, streets lighting, large spaces for sporting or entertainment events, and in transport for lighting and signaling, both on land or sea or air [1, 2]. The power density featured is very variable and depends on the type of application and ranges from a few Watts to thousands of Watts. Furthermore, the power source can be different from direct current (DC source) to alternating current (AC source), presenting different needs for interfacing with Solid-State Lighting (SSL) [3]. In the lighting scenario, a LED light system (light bulb, street-light, floodlight and so on) can be considered as a combination of LED semiconductor materials and a driver circuit.

LED light system is acknowledged as the actual generation of the sustainability light source. It has many benefits compared with incandescent lamp and the fluorescent lamp [4–7]. It features high efficiency, long life, safe and environmental

protection, small size, high reliability and fast response speed. In the last generation of the LED light bulbs, the equivalent lighting effect is achieved with power consumption about 1/10 of incandescent lamp and 1/2 of the fluorescent lamp [8].

The design of the LED driver circuit plays a key role to achieve a performant light system. The light brightness is function to the supplied forward current. Therefore, LED is a current-driven device. The driver circuit must provide the correct level of current for the required brightness as well as comply with other characteristics such as:

- high reliability, necessary in cases of operation in difficult conditions (for example in transport at very low temperatures or generally, for continuity of service needs),
- high efficiency to reduce losses and improve performance and autonomy in the case of portable lighting systems with batteries as a source,
- small volumes of the power converters for arranging the drive circuits to meet the demands of having LED bulbs, light fixtures, and modern lighting systems as compact as possible,
- flexibility and precision in control to adjust the brightness to avoid phenomena such as flicker with the fault-tolerant capability,
- surge protection necessary due to the vulnerability of light emitter diodes to over voltages and low resistance to reverse voltages (for example, high voltage spikes from the power grid can occur in LED streetlights),
- additional protection functions such as input under-voltage, temperature or short circuit of converter power switches,
- high power factor (PF), in the case of AC power supply with a satisfactory power quality waveform and consequently with low Electromagnetic interferences (EMI) contents.

Specifically, in AC connected LED driver a high PF leads a displacement power factor next to one and an input current with quite low total harmonic distortion (THD) [9, 10]. Furthermore, the LED light system must comply with the national and international standards and regulations concerning harmonic currents, such as the standard IEEE-Std-519 and the IEC 61000-3-2.

Other characteristics of the driver circuits concern the circuit structure. The circuits solutions can be passive or active topologies. Active circuits can be classified as linear or switching type. Furthermore, the driver circuits can be non-isolated if the output current is limited and a low voltage source is involved or can be isolated when the safe operative conditions are prevalent and a higher output current is requested [11]. Additionally, the information and communication technologies (ICT) are making the driving of solid-state lamps smarter and smarter, allowing to vary the brightness level (dimming) and the colors through remote and controlled communication systems by means of user interfaces developed according to the needs of the user [12].

This chapter is organized as follows.

In the Section 2, the basics of the LED driver are addressed. Furthermore, the main passive, and active circuit for the solid-state lighting driving are described and classified.

In the Section 3, the main topologies of the DC-DC switching driving circuits are presented and analyzed.

In the Section 4, the switching-type driving circuits and their interfacing with the network AC and DC source are investigated.

## 2. LED driver circuit basics

In an LED device the emitted light follows the increment of the current. It is almost proportional to the supplied current. However, the relationship between voltage and light output is highly nonlinear. The direct voltage  $V_F$  drop and the current  $I_F$  are linked by an exponential function typical of the silicon diode. In **Figure 1a** the voltage–current characteristic is depicted for a white LED. The curve has been obtained by a variable voltage source with series resistance to control the diode direct current. In **Figure 1b** the circuit schematic of the LED characterization is shown. From the **Figure 1a**, the diode features rated voltage of 3.5 V and a rated current of 700 mA, while the threshold voltage  $V_{th}$  is 2 V. From **Figure 1b** the resistance  $R_S$  to obtain the requested current is

$$R_S = \frac{V_S - V_F}{I_F} \quad (1)$$

The circuit schematic of **Figure 1b** is also the basic linear LED brightness control. Referring to **Figure 1a** two control approaches can be performed. In the first methodology, the LED V-I curve is used to set the voltage needs to generate the requested forward current. In the second driving approach, the LED device is controlled with a constant-current source to drive the LED eliminating the high current changing due to little variations in forward voltage control. Indeed, the high slope of the voltage–current curve leads that a small change of voltage that can carry on a significant change of current through the diode consequently, a considerable change of the emitted light appears. To avoid any flickering, LEDs need a constant current source [13]. Furthermore, constant current control circuits are robustness for the load short-circuit but suffer the load fully open conditions.

The LEDs can be driven by different kind of passive or active circuits. Furthermore, the active driver circuits can be classified in linear or switching topologies.

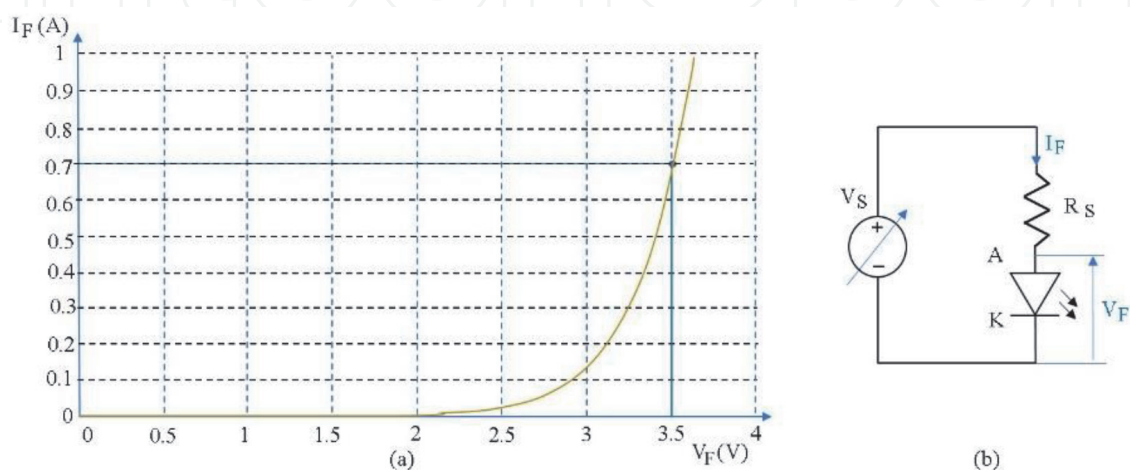
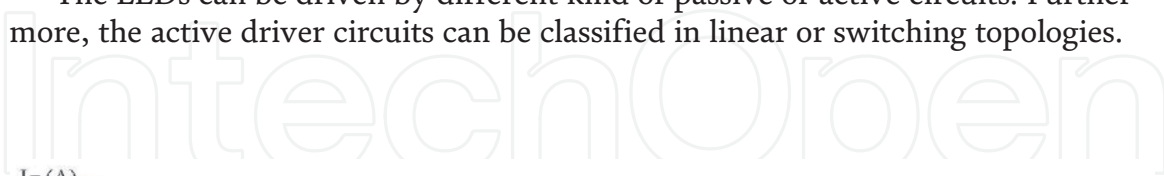


**Figure 1.**  
 (a) I-V curve characteristic for a white LED, (b) schematic of characterization circuit.

## 2.1 Passive drive circuits

The quantities of current and voltage to be supplied to the LED to achieve the required brightness can be provided with different circuits. Passive LED drivers feature the exclusive use of passive components (e.g., resistors, capacitors, magnetic components) and silicon diodes. The simplest and most reliable circuits are passive ones. This simple and cost-effective circuits do not exhibit performance like linear or switching driver circuits and operate without precise control of the output current. They generally provide a DC current with AC current ripple but are still used in those cases where reliability and continuity of service are prevailing parameters comparing to dynamic performance and efficiency. Examples of applications are outdoor street-lights that operating in difficult environmental conditions where complex circuits can be more vulnerable. Use of an impedance between the ac line and the LED light bulb load to fix and limit the current is mandatory. The main drawbacks of these passive topologies are the low PF and THD featured, sometimes not enough to comply with the standards [14]. Passive LED drivers can be arranged in two main categories, lossy and lossless (ideal) passive circuits [15].

The lossy passive driver is usually composed of a transformer that lowers the mains voltage to one compatible with the number of LEDs to be driven (The load is generally composed of LED arrays), a bridge rectifier circuit which rectifies the alternating voltage, an electrolytic capacitor which reduces the AC ripple and finally a resistor in series with the LEDs. The current limitation is achieved by means of a simple resistor. In some LED driver applications, a linear circuit replaces the resistor [16]. The traditional passive circuit described is represented in **Figure 2a**. The step-down transformer reduces the voltage drop on the resistor  $R_S$  leading to an increase in the overall system efficiency. Furthermore, the transformer guarantees galvanic isolation. A large electrolytic capacitor  $C_S$  is used to reduce the ripple appropriately in order to avoid flickering. The large value of  $C_S$  necessary lead to pulsating input currents which high harmonics contents. Generally, the PF of such circuits is low and hardly is comply with the Class D limit [17].

In this type of passive driver, the main cause of the efficiency reduction is the conduction losses of the  $R_S$  resistor.

The “lossless” drivers use to limit the current of the LEDs ideally a lossless impedance (such as inductors and capacitors). An inductor positioned on the AC side can be used to limit the current as shown in **Figure 2b**. The inductor  $L_{in}$  produces an impedance that withstands the voltage difference between the input voltage  $V_{AC}$  and the output voltage  $V_0$  required across the LEDs. The  $L_{in}$  impedance does not require the step-down transformer of the previous circuit solution. Furthermore,  $L_{in}$  acts as an input filter. As consequence on the DC side, after the rectifier bridge, it is possible to use a capacitor  $C_S$  with a smaller capacity and therefore not electrolytic. The use of non-electrolytic capacitors allows a long life of the entire system. The  $L_S$  on the DC side is used to convert the rectifier output

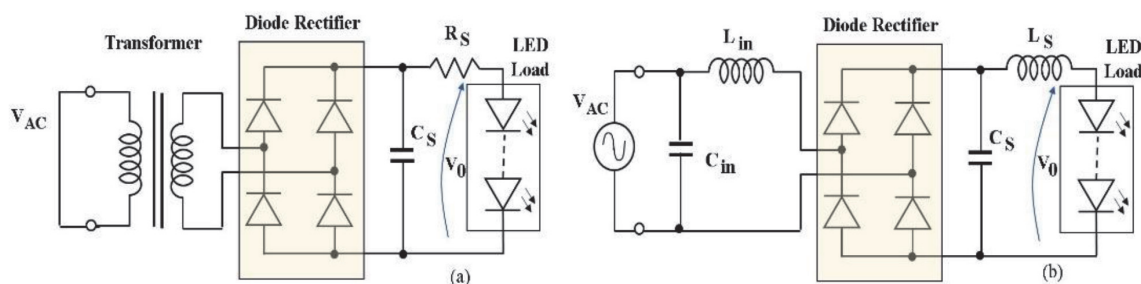


**Figure 2.** Passive LED driver circuit. (a) Lossy passive circuit, (b) lossless passive circuit.

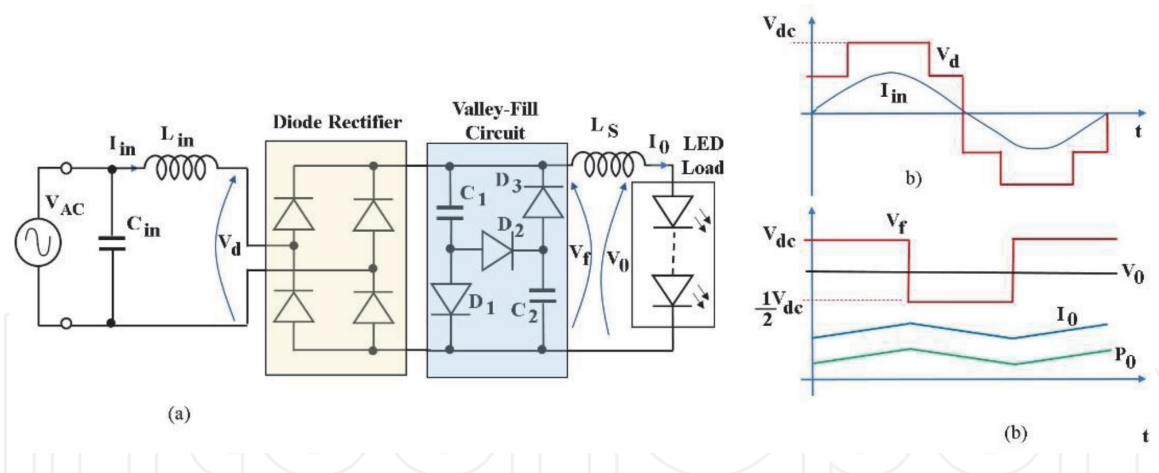


**Figure 3.**  
 (a) Passive driver circuit with valley-fill circuit. (b) Idealized waveforms of circuit operation.

voltage into a direct current source  $I_0$  to drive the LED load. The input capacitor  $C_{in}$  is useful for further improvement of the input power factor. The use of a power factor correction capacitor  $C_{in}$  is a standard method used in the magnetic ballast in the case of fluorescent lamps [18].

A passive driver circuit using the Valley-fill topology is depicted in **Figure 3a**. The Valley-fill circuit has been widely used in ballast systems for powering gaseous discharge lamps. It allowed having a power factor of 95% without the need for additional control [19]. In the case of LED diode drivers, Valley-fill enhances the improvement of the ripple of the output voltage, maintaining an adequate quality of the current waveform at the input thanks also to the presence of the  $L_{in}$ . Also in the Valley-fill circuit the capacitors used are not electrolytic. The idealized waveforms of the main input and output voltages together with the power  $P_0$  are shown in **Figure 3b**. The analysis of the presented waveforms is reported in detail in [20].

## 2.2 Active drive circuits

In low power applications, linear regulators are used extensively. As power increases due to losses, these regulators are replaced by current regulated switching converters. In many applications, the LED diodes in single or in string configuration are used as indicators (smart home devices, LED displays, rear lights, directional lights in the automotive sector, animated LED circuits, etc.) with linear regulators using dedicated integrated circuit (IC) devices.

The principle of operation of a linear regulator is shown in **Figure 4a**. the necessary constant current is established by means of feedback through a sensing resistor and a comparator circuit which compares a reference voltage with the actual voltage on the sensing resistor. The necessary LED current is established by the relation (2).

$$I_{LED} = \frac{V_{REF}}{R_S} \quad (2)$$

This type of regulator is usually realized in an integrated way. The integrated solution is more attractive because reduces board space and component count, simplifying circuit and system designs [21]. In **Figure 4b** the application circuit of an integrated regulator (IC) with battery source (NUD4001 - On-Semiconductor) for driving up to 500 mA of a LED strings is shown [22].

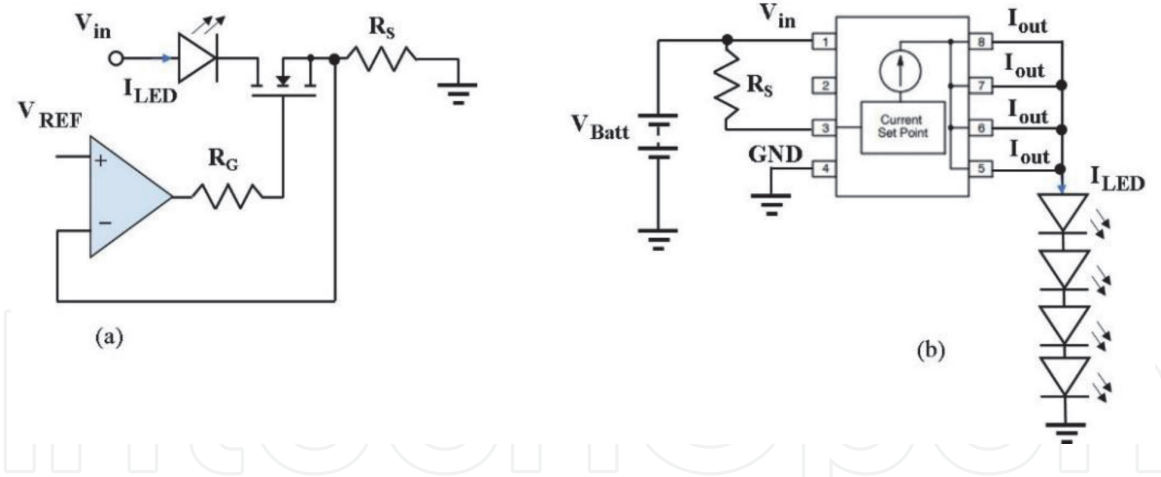


**Figure 4.** (a) Operation principle of a linear regulator LED driver. (b) Schematic of actual IC (NUD4001) for a string LED driver applications.

Driver topology	Current control method	Advantage	Disadvantage
Passive	Resistor	<ul style="list-style-type: none"> <li>• Easy design procedure</li> <li>• Low cost</li> </ul>	<ul style="list-style-type: none"> <li>• Not accurate current control</li> <li>• High power dissipation on the resistor for high power LED</li> <li>• Low Efficiency with increasing LED power request</li> </ul>
Active Linear	Linear control loop	<ul style="list-style-type: none"> <li>• Accurate current control</li> <li>• Capability of dimming by current control</li> <li>• do not require electromagnetic interference (EMI) filters</li> </ul>	<ul style="list-style-type: none"> <li>• High power dissipation with heat-sink need with increasing LED power request</li> <li>• Lower efficiency</li> </ul>
Active switching	PWM current control	<ul style="list-style-type: none"> <li>• High efficiency</li> <li>• Dimming capability by PWM control</li> </ul>	<ul style="list-style-type: none"> <li>• More complex design</li> <li>• Higher cost</li> <li>• EMI design constraint</li> </ul>

**Table 1.** Design constraint comparison for passive and active driver circuits.

The ever increasing demand for LED systems with high brightness and improved energy efficiency, especially for portable power applications, has led to the introduction of more and more advanced switching LED current control drivers with various features and better current matching/regulation. The use of power devices in switching operation allows to overcome the limits of linear regulators regarding efficiency [23]. Furthermore, the increasing switching frequency of the last generation power devices allows using inductor and high-frequency (HF) transformer with reduced core size featuring compact volume [24]. Several converter topologies are available depending on the power range and other characteristics such as galvanic isolation need, size and cost-effectiveness, easy dimming capability, modular approach availability and efficiency target. In switching converters, the current and voltage control is achieved by pulse width modulation (PWM) strategy. In a battery source, the switching LED driver is effective in the management of multiple LED strings and array in several kinds of application such as in automotive or in portable electronics devices [25]. The main design features of switching driver circuit with pros and cons compared with linear and passive solutions are reported in **Table 1**.

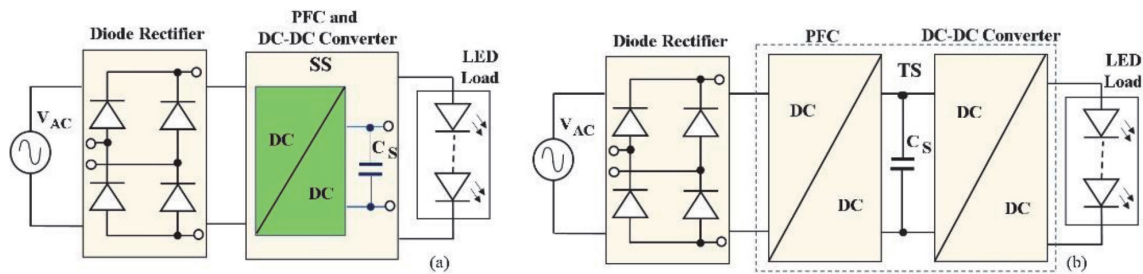


**Figure 5.**  
 (a) SS switching driver block schematic. (b) TS switching driver block schematic.

In the AC source the switching LED drivers are used specially in indoor application. For the topologies attached to the electricity grid, the power factor plays a crucial role. Two solutions are pursued. In the first solution, the PFC can be composed within a single stage together with the actual driving circuit. In this case, it is referred to as a single-stage driver (SS). The SS driver block schematic plus the filter capacitor  $C_S$  are reported in **Figure 5a**. In the SS driver circuit, the filter capacitor is usually connected after the DC-DC converter, which is on the high-frequency side to obtain a high PF [26, 27]. In the second approach, the driver topologies have a two stage (TS). The first stage is a front-end PFC converter and the second stage is a DC-DC converter which controls the requested current in a string of LED [28]. In **Figure 5b** the block schematic of a TS driver is depicted. In TS driver the filter capacitor is placed between the two semi-staged downstream from the PFC DC-DC converter to obtain high PF. SS drivers arrangement can significantly increase efficiency by dramatically reducing component cost and volume at the expense of more complex control. In the case of light bulbs of reduced power and small dimensions, single-stage topologies are certainly to be preferred. The TS solution provides accurate and flexible control also with dimming feature of the DC-DC converter separated by the PFC control design at the expense of additional circuitry and cost. Furthermore, with the second stage DC-DC converter, is possible the use of a not electrolytic capacitor. The second stage compensates the low-frequency ripple on the output voltage to achieve an AC-DC LED driver with a lifetime comparable to that of the LED devices. In the range of medium power, SS or TS topologies choice depending on the trade-off of the design constraints. Generally, TS approach is suitable in higher power applications.

In case of industrial environment and higher power request for high-brightness Light-Emitting Diodes (HB-LEDs), three-phase AC source can be supplied. In these applications three phase rectifier can be used to power the DC-DC converter. In three-phase AC source also a multi-cell converter solution may be used. In this topology approach, three single-phase converters in a star or delta connection to the three-phase power grid are arranged and linked in parallel connection at the output [29]. Finally, in **Figure 6a** block diagram classification of ac-dc LED drivers for both single-phase and three-phase AC source are summarized.

### 3. DC-DC converter topologies for LED driver circuits

The LED driver circuits topologies selection depending on three basic needs. The kind of energy sources (DC or AC), the power requirement and the galvanic isolation features. In the following, as the first study case, the converters for DC sources are investigated.



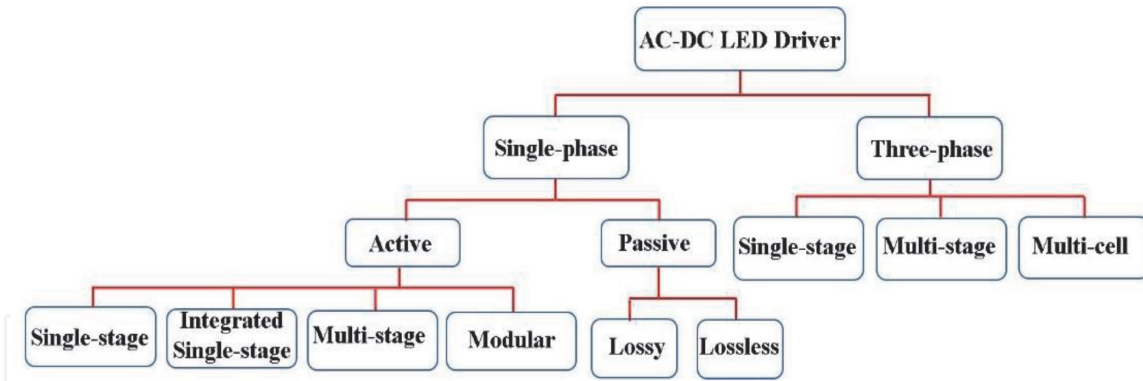


**Figure 6.**  
Block diagram of AC-DC LED driver circuits classification.

### 3.1 DC-DC converter circuits

LED drivers often require step-up/step-down regulation DC/DC converters. The power converters supply constant current at a voltage from a not constant input voltage (actual battery source). The battery source voltage can be higher or lower than the load request. The converter output voltage can be regulated by the power switch duty ratio modulation strategy (PWM), taking into account a feedback adjustment by the output current [30]. Considering a single switch converter, a simple buck converter is a basic topology for the voltage and current control of the LED string (**Figure 7a**). It enables simple, efficient and cost-effective solutions for driving regular and high-brightness LEDs. In steady-state the duty cycle regulates the output voltage by the duty cycle ( $d$ ) duration (3).

$$V_0 = d \cdot V_{in} \quad (3)$$

Multiple LEDs solution need an adequate voltage amount. Step-up (boost) LED drivers acting with a current control achieving a higher load voltage of the DC source available (**Figure 7b**). In this step-up converter, in steady-state conditions, the output voltage is higher than the input voltage as described by

$$V_0 = \frac{1}{1-d} V_{in} \quad (4)$$

In case of a wide input voltage range, a buck-boost topology is preferable. In the buck-boost converter, the output voltage is regulated by

$$V_0 = \left| \frac{d}{1-d} \right| \cdot V_{in} \quad (5)$$

In this converter the output voltage has an opposite polarity than the input voltage (**Figure 7c**). Furthermore, the diode  $D_S$  and  $C_0$  in the output stage can provide an LED short circuit protection feature. This circuit property, for example, is very crucial in automotive applications.

An improving alternative is the Ćuk converter. It is composed of a boost converter followed by a buck converter. As the buck-boost, it is suitable in applications where an input voltage from a continuous source (e.g. battery) can be greater or less than the requested output voltage. It maintains the same regulation law at steady-state of the traditional buck-boost converter with inverted polarity in the output voltage. The Ćuk converter features some benefits compared with the buck-boost converter in the matching of the LED driver design constraint. The topology

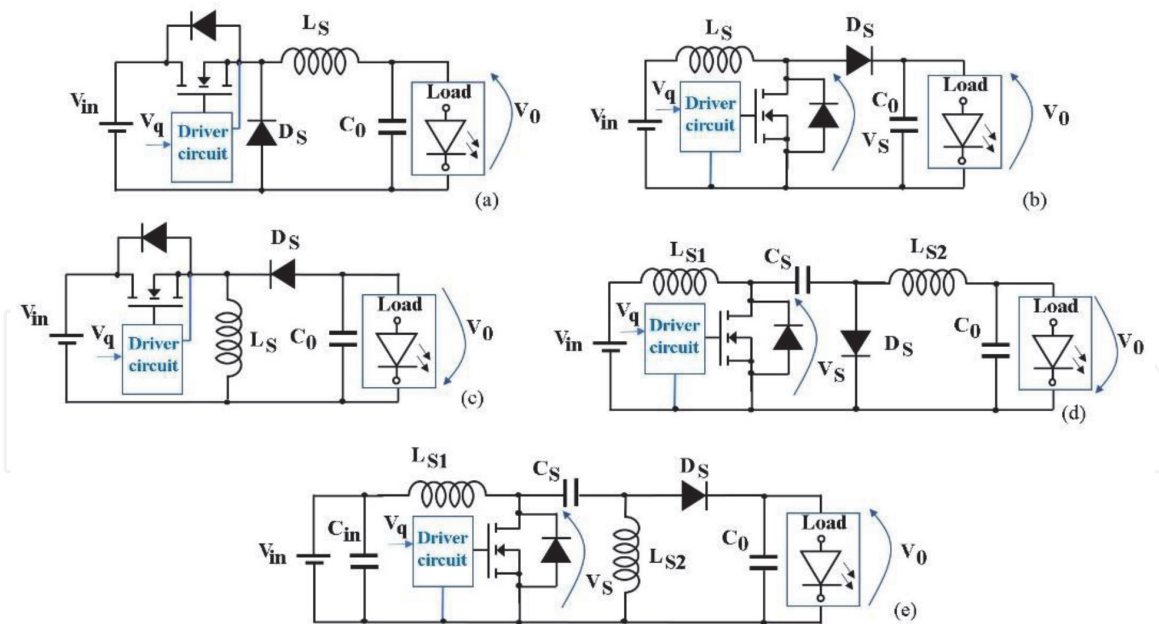


**Figure 7.** Non isolated converter for LED driver circuits. (a) Buck converter (b) boost converter, (c) Buck-boost converter, (d) Cuk converter, (e) SEPIC converter.

structure achieves low input and output current ripples [31]. The presence of an inductor in the input stage of the circuit allows a smoothed input current waveforms. Furthermore, the LC filter in the output stage facilitates a smooth current waveform (**Figure 7d**). Moreover, this converter has four energy storage devices (two inductors and two capacitors) which can provide higher output power compared to other converters such as buck, boost and buck-boost of the same electrical characteristics. The disadvantage of this topology is a higher number of passive components and more complex control. Another interesting topology is the SEPIC converter [32]. It has the advantages of low input current ripple achievement due the presence of the LC filter in the input stage (**Figure 7e**). Furthermore, the output voltage is not inverted polarity. The drawbacks are as a Cuk converter the higher number of passive components and more complex control due to fourth order dc-dc converter transfer function. Moreover, SEPIC converter has a higher voltage stresses on the power switch.

$$V_S = V_{in} + V_0 \quad (6)$$

To reduce the current ripple every converter described usually operated at constant current mode (CCM) and the power rate of these converter applications is up to about 150 W.

### 3.2 Current control in LED driver DC-DC converter circuits

A basic control system to reach the requested LED brightness a peak current control (PCC) is widely used for drive based on Buck, Boost and Buck-Boost converter topologies. In the following, for simplicity, the Buck converter control strategy is investigated, but the considerations that will be made can be easily extended for the other topologies already described. In the Buck converter, the current sensing resistor can be connected to the source of MOSFET devices (**Figure 8a**). In this way, the current is only sensed during the on-state of the MOSFET switch compared to the sensing resistance located in load side, reducing power losses. Generally, the Buck converter topology can be rearranged in a

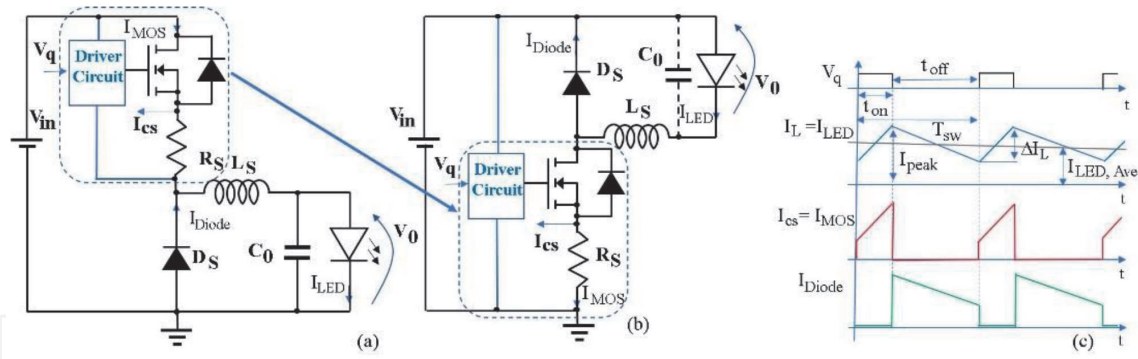


**Figure 8.** Buck converter with MOSFET with the sensing resistance layout arrangement in the traditional in (a) high-side location and in (b) low-side position. (c) Switching waveforms of command signal  $V_q$  and the main converter currents.

different way to reduce the noise signal, positioning the sensing resistor with a pin to ground (**Figure 8b**). The capacitor  $C_0$  in some industrial application, in low side MOSFET solution, is removed as highlighted in **Figure 8b** (LUMILED HB-LED arrangement) [33]. The main switching current waveforms and the gate control voltage  $V_q$  in steady state conditions are reported in **Figure 8c**.

The operating principle of the PCC control is shown in **Figure 9** in the condition with the low-side MOSFET and the sensing resistor between source and ground.

The current control works as follows. The clock signal leads the control signal  $V_q$  high and the current in the inductor ramps up. When the transduced MOSFET current  $I_{cs}$  reaches the reference  $I_{peak}$ , the comparator resets the command signal and at the next clock signal, the control cycle is repeated [34]. The schematic of the PCC control is depicted in **Figure 9a**. The main control waveforms and the LED current are reported in **Figure 9b**. From **Figure 9b** the current ripple,  $\Delta I_L$ , is evaluated by:

$$\Delta I_L = \frac{V_{in} - V_0}{L_S} t_{on} = \frac{V_0}{L_S} t_{off} \quad (7)$$

The average LED current  $I_{LED,Ave}$  can be calculated as

$$I_{LED,Ave} = I_{peak} - \frac{\Delta I_L}{2} = I_{peak} - \frac{V_0}{2L_S} t_{off} \quad (8)$$

$$I_{LED,Ave} = I_{peak} - \frac{V_0 T_{sw}}{2L_S} \left(1 - \frac{V_0}{V_{in}}\right) \quad (9)$$

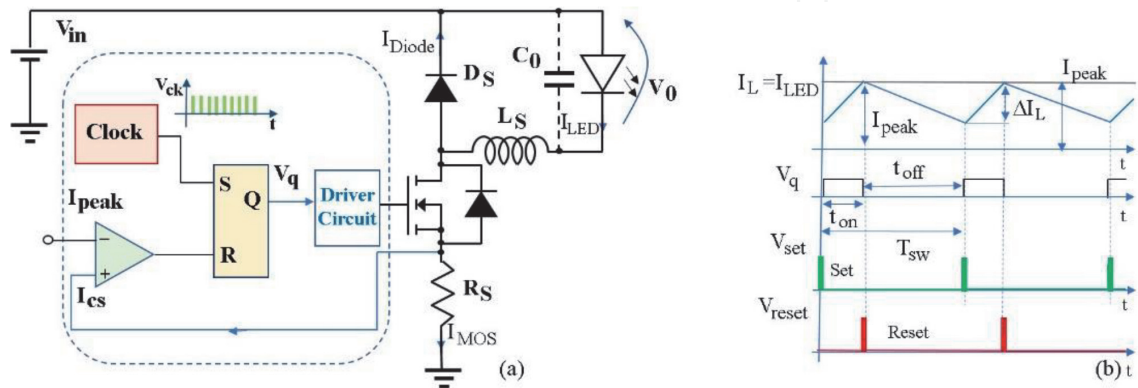


**Figure 9.** Peak current control technique (a) circuit schematic of the control method and Buck in low side MOSFET solution. (b) Main control signal and led current behavior.

As demonstrated in (9) the LED current depends on  $V_{in}$ . A large variation of  $V_{in}$  affects the  $I_{LED,Ave}$  losing control accuracy with respect to the  $I_{peak}$  reference.

A more accurate control should contain compensation for the variation of the input voltage  $V_{in}$  in order to keep the LED current closer to the reference value  $I_{peak}$ .

The CPM technique achieves the following advantages

- Simply control circuit implementation and robust;
- Constant switching frequency strategy, with constant switching losses.
- Intrinsic short circuit protection. MOSFET failure for over current can be controlled by limiting the maximum reference current;
- In converter application with isolating transformer, the saturation problems can be reduced;
- Easy LED driver module application capability. The modules can be connected in parallel with equal current sharing providing equal current control for each module.

As disadvantages have

- Susceptibility to noise;
- Sensitive to the wide  $V_{in}$  variation.

Finally, the current regulation of LED to obtain a dimming effect combine the PCC strategy and an adjustable PWM signal. A conventional circuit structure is shown in **Figure 10**.

To avoid inaccuracy in the controlled current a hysteresis-current control (HCC) technique can be implemented. In HCC strategy is necessary to control the on and off current value. The controlled current is always included within a defined hysteresis band [33]. In this control solution, the sensing resistor can be positioned in series to the LED, thus the high-side MOSFET buck layout may be used, as shown in **Figure 11a**, to allocate the sensing resistor with a grounded pin [35]. The sensing

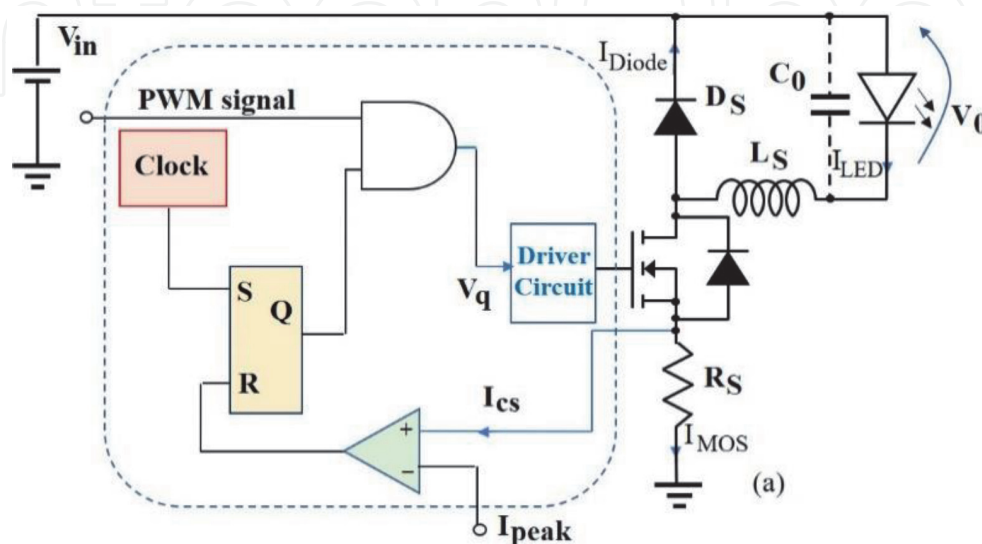


**Figure 10.** Schematic of driver circuit with PCC strategy combined and PWM control signal to act the dimming effect.

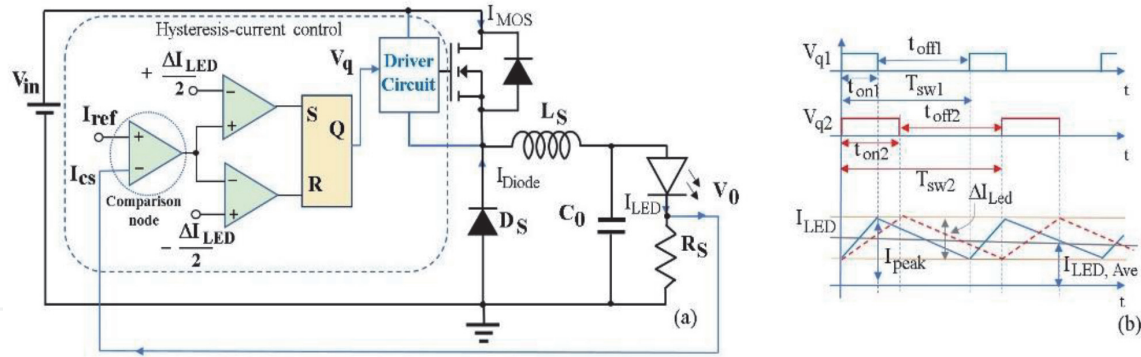


**Figure 11.** (a) HCC control scheme in high-side MOSFET Buck converter. (b) The controlled current behavior with a fixed hysteresis band in two different cases of the control signal  $V_q$ .

current is compared with a reference current and the error is forward to a window detector with the band levels positive and negative requested. The controlled current behavior with a fixed hysteresis band in two different cases of the control signal  $V_q$  is reported in **Figure 11b**. The HCC technique is non-constant frequency control.

The advantages of this control strategy are

- Fixed band hysteresis control does not present stability problems
- low software requirements in digital form implementation,
- high reliability, and less tracking error.

The main disadvantage is the non-constant frequency control. It means a switching losses variable and generally higher compared with the previous control method. But with the new generation of wide-bandgap devices such as GaN, the switching losses are strongly reduced and this control method is more attractive [36].

A further hardware arrangement to achieve switches losses reduction in buck converter is the use of a MOSFET (or GaN) devices to replace the diode  $D_S$  working in a synchronous way with the high-side switch [36].

### 3.3 Higher power LED driver DC-DC converter and galvanic insulation feature

As the power required for driving LEDs increases, more complex topologies and galvanic isolation is required to isolate the DC source from the LED strings, increasing safety and protection against short circuits on the load side. In the field of medium power (up to about 100 W) the Flyback topology is usually the one most used for the reduced number of components, low cost, together with efficiency even above 90% (**Figure 12**). The increase in efficiency depends on the type of switch selected, whether pure silicon or wide-bandgap devices [37]. The presence of two inductances coupled to transfer energy between the primary side and the secondary side allows the galvanic isolation required in many applications. The Flyback converter is an isolated arrangement of the Buck-Boost converter. The output voltage depends on the ratio of the number of windings on the primary side and secondary side and maintains the Buck-Boost converter duty cycle dependence (10).

$$V_0 = \frac{N_s}{N_p} \cdot \frac{d}{1-d} \cdot V_{in} \quad (10)$$

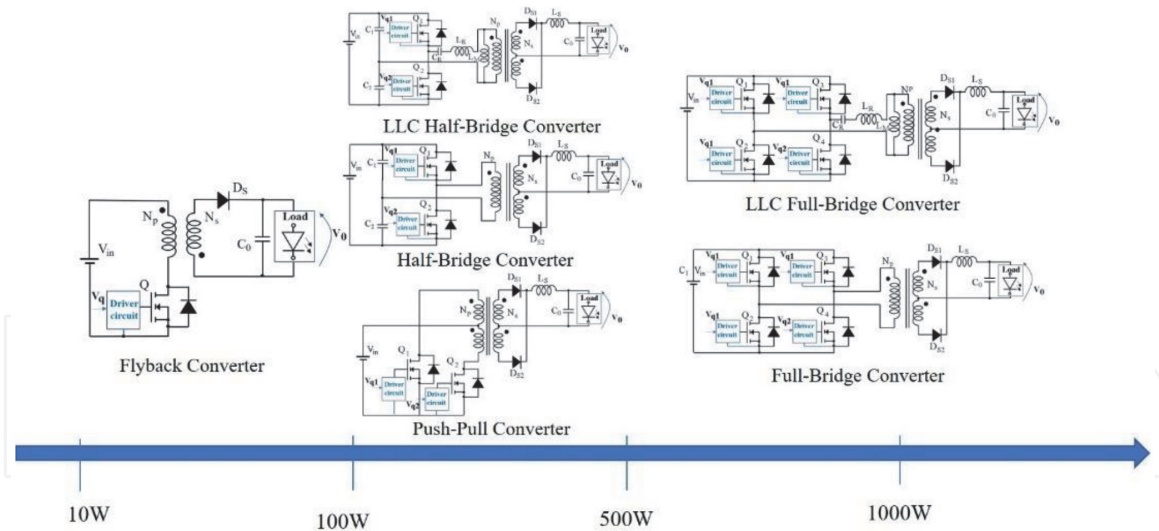


**Figure 12.**  
 A qualitative estimation of the isolated application versus the power rate.

It works with a DC power supply and therefore falls within the classification outlined. Usually, the Flyback converter is used attached to the grid to create single-stage AC/DC drivers, thus it will be more fully discussed in the next session.

In the Flyback converter, the single switch use limits the power rate. Furthermore, a single switch does not make the best exploitation of the magnetic hysteresis loop, producing losses in the magnetic core [38]. In the field of higher powers, topologies based on Half-Bridge, Push-Pull and Full-Bridge converter are applied to supply high current. These converters all have high-frequency transformers that allow galvanic isolation. The high switching frequencies used (around hundreds of kHz with wide-bandgap devices) achieve a transformer volume reduction. An additional advantage of the transformer is the availability to feature several secondary windings. Therefore, several LED strings can be supplied at the same time also with different strings arrangement. The Half-Bridge converter (**Figure 12**) has the following transfer function

$$\frac{V_0}{V_{in}} = \frac{N_s}{N_p} \cdot d \quad (11)$$

To avoid devices cross conduction, the duty cycle must be  $d < 0.5$ . It has the following pro and cons.

Pro: better transformer utilization, best application up to 500 W, single winding primary, switch voltage limited stress (equal to  $V_{in}$ ).

Cons: hard switching operation, floating driver circuit need for the high side MOSFET, high primary current stress.

The Push-Pull converter operates in hard switching at  $d < 0.5$ . It has the same transfer function of the Half-Bridge converter multiplied by 2. In the Push-Pull converter the MOSFETs driver circuits are more simple because there are two switches in low side position (**Figure 12**). Push-Pull topology features lower input ripple than the Half-Bridge. On the other hand, at turn-off the switches have higher voltage stress are  $(2V_{in})$ . Furthermore, in the primary side the transformer is center tapped [39].

The Full-Bridge structure is composed of four switches (see **Figure 12**). It has a twice transfer voltage ratio as the Half-Bridge topology and operating with  $d < 0.5$ . It features twice the power rate than the Half-Bridge solution with equal MOSFETs voltage stress (equal to  $V_{in}$ ), but it has a more complex structure.

To reduce power losses with increasing efficiency, in higher power driver converter topologies, solutions with soft switching operation have been increasingly used. In these circuit types, the LLC resonant converter in half-bridge and full-bridge topologies are the most studied and applied [40]. The LLC resonant converter operation will be better discussed in the next section.

In **Figure 12** qualitative estimation of the isolated power converter topologies versus the output power rate are shown.

#### 4. AC connected switching LED driver circuits

LED driver circuits connected to the grid must meet several requirements regarding the frequency and the quality of the waveforms that are linked to the grid. The power factor must be controlled by means of a dedicated PFC circuit. Furthermore, it is necessary to keep the levels of Electromagnetic Interference (EMI) contents introduced into the grid low. Also, the flicker limits for LEDs must be considered.

In the design of drivers connected to the electrical network, before finding the circuit solutions it is essential to know the regulations and recommendations that an LED driver must comply with. The following design rules and standards must be taken into consideration.

- the ENERGY STAR® program recommendations, with specific regulations and requirements for LED lighting equipment [41],
- the harmonic standard (i.e. IEC 61000–3-2),
- flicker rules and metrics [14].

To observe the design constraints, the driver circuit is composed of several modular blocks. Each block meets certain requirements. In **Figure 13**, the schematic of the LED driver for an AC lighting system is reported. From the line to the load (LED strings), there are the EMI filter, the diode rectifier, the PFC and the DC-DC converter. This schematization has been referred to as a dual-stage driver. If the power factor correction is integrated into the control in the DC-DC converter, then it is referred to as a single-stage driver.

##### 4.1 Flyback single stage LED driver circuit

The single-stage LED driver is very attractive. On the other hand, it has to combine the control both the PF and the current to be supplied to the LEDs. The topology widely used in these applications is the Flyback converter especially at power rates below 100 W. The structure of the Flyback converter has the least

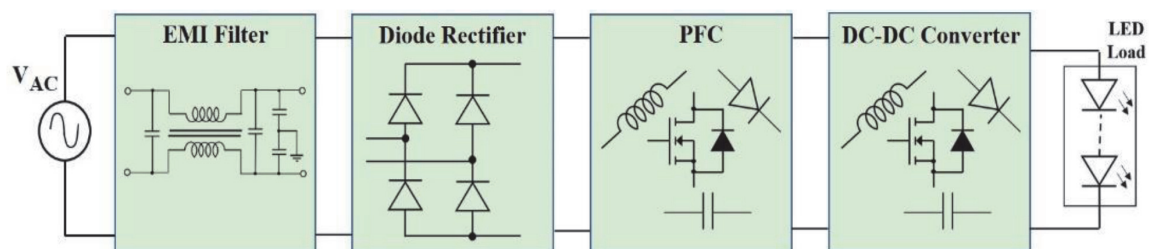


**Figure 13.**  
Blocks schematic of a AC source LEDs driver circuit.

components compared with other isolated converters, and many studies have been conducted on the grid connection to obtain high PF and low THD [42, 43]. In the LED driver application, the operative conditions usually used is a critical conduction mode (CRM) or the discontinuous conduction mode (DCM) [44]. In DCM (or CRM) the switch turn-on can be driven when the transformer is completely demagnetized, thus transformer saturation is avoided. The efficiency of the Flyback converter can be increased using the soft-switching technique exploiting the parasitic components present in the structure of the converter and of the power switch (**Figure 14a**). The quasi-resonant (QR) mode is used in the Flyback application to reduce the switching losses despite the non-constant frequency operation. Moreover, the QR operation allows has an enhanced transient response in DCM operation and it features a smaller EMI filter [45].

In addition, the QR Flyback LED driver has higher safety properties under output short circuit conditions. In the QR operation, the MOSFET is not turned on until the primary windings are fully demagnetized. On the other hand, a high ripple output current and high output diode and switch conduction losses in comparison to the fixed frequency driver. A further drawback well know is the high voltage stress on the switch given by

$$V_{DS,peak} = V_{in} + \frac{N_p}{N_s} V_0 + V_{stray} = V_{in} + V_r + V_{stray} \quad (12)$$

Where  $V_r$  is the output voltage reflected in the primary side and  $V_{stray}$  is the peak voltage of the ringing at turn-off transient due to the equivalent primary inductance  $L_{ps}$  and the equivalent parasitic capacitance ( $C_{ps}$ ) composed by the output MOSFET capacitor and the equivalent primary side stray capacitor (**Figure 14a and b**). The resonant frequency  $f_{rs}$  is

$$f_{rs} = \frac{1}{2\pi\sqrt{L_{ps} \cdot C_{ps}}} \quad (13)$$

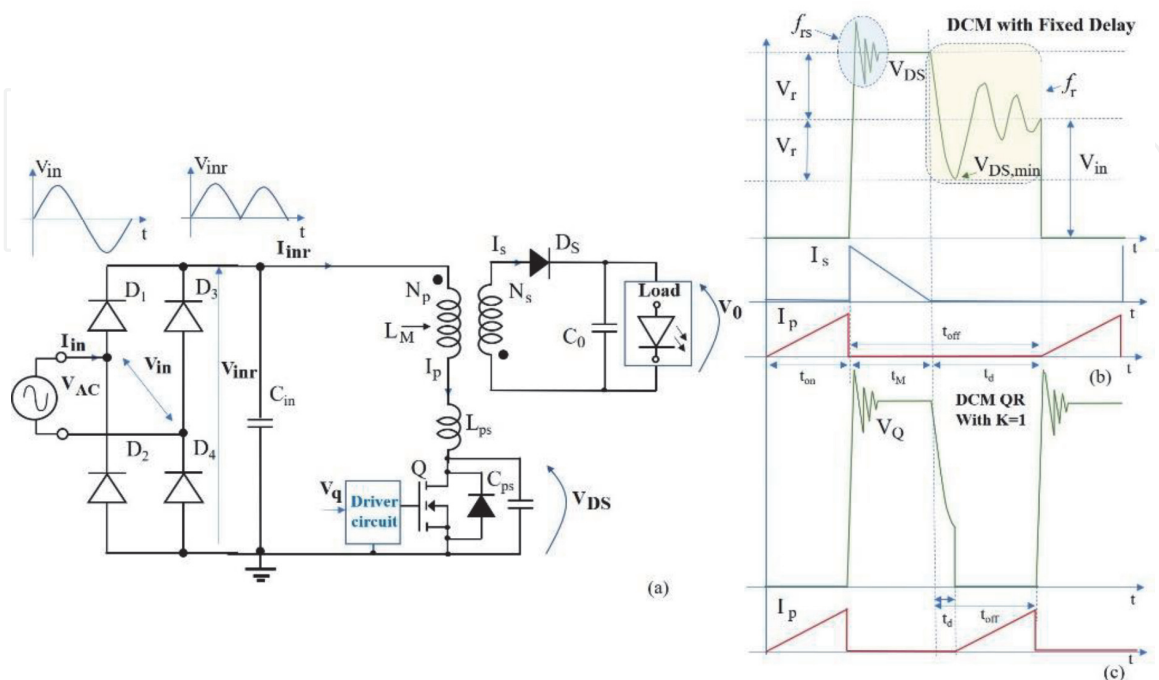


**Figure 14.**  
 (a) Schematic of Flyback converter with the stray inductance and capacitance reported on the primary side.  
 (b) DCM operation at  $t_d$  constant. (c) DCM in QR operation with  $k = 1$ .



In a DCM traditional operation flyback converter, the gate driver acts with a constant switching frequency, while in a QR operation a variable frequency is featured [46]. To turn on the switch a demagnetization time  $t_M$  is necessary. After  $t_M$ , a natural oscillation typical of a second-order system appears. The resonant frequency  $f_r$  is lower than  $f_{rs}$  and is related to the equivalent primary inductance  $L_p$  composed by the magnetization inductance  $L_M$  and the equivalent stray inductance on the primary side  $L_{ps}$  with the equivalent parasitic capacitance.

$$f_r = \frac{1}{2\pi\sqrt{L_p \cdot C_{ps}}} \quad (14)$$

A simplified Flyback converter with the stray inductance and equivalent parasitic capacitor on the primary side linked to the AC source by a rectifier bridge is depicted in **Figure 14 a**. In DCM operation at a constant frequency, a constant delay time  $t_d$  is added to  $t_M$  to compose the turn-off time. In QR operation a resonant valley detection achieved by the control circuit is provided to switching at lower power losses. **Figure 14b** depicts the drain-source voltage waveforms and the current both in the primary and secondary side in DCM with constant frequency operation and QR operation with the turn-off at the first valley (**Figure 14c**).

The switching period  $T_{sw}$  is

$$T_{sw} = t_{on} + t_M + t_{osc} \quad (15)$$

Where  $t_{osc}$  is the complete ringing time for the  $V_{DS}$

$$t_{osc} = \frac{1}{2} [1 + 2(k - 1)] \frac{1}{f_r} \quad (16)$$

As reduced load  $t_{on}$  is reduced yet. At light load, the switching frequency is higher. Also, the ringing time  $t_{osc}$  increase with the decrease of the load [47]. The quantitative  $k$  specifies the number of rings within  $t_{osc}$ . Even, the number  $k$  is inversely proportional to the load. The control strategy acts considering the  $k$  to detect the better valley point to turn-off. At light load, the controller can be operated considering  $k$  different from 1 because the losses are still reduced. At high load, the  $k$  usually considered is equal to 1 to reduce drastically the losses.

## 4.2 Control method to obtain high power factor

The market requirements are based on standard IEC61000-3-2. It defines some input current THD targets (e.g., <10% at full power) that are very difficult to achieve, especially when working with lighting equipment over 25 W.

As know, the distortion corresponding to the harmonics contents. The distortion power factor DPF in the hypothesis of a perfectly sinusoidal input voltage is

$$DPF = \frac{1}{\sqrt{1 + THD_i^2}} = \frac{I_{in1,rms}}{I_{in,rms}} \quad (17)$$

Where  $THD_i$  is the input current total harmonic distortion. The current  $I_{in1,rms}$  is the baseband component of the current, while  $I_{in,rms}$  is the total input current. The true Power Factor (TPF) in non-linear grid load such as the power converter is related to the Distortion Power Factor and the Displacement Power Factor.

The Displacement Power Factor is due to the phase shift between voltage and current at the fundamental line frequency. It is defined as the ratio between the real

power average  $P_{ave}$  and the apparent power in perfect sinusoidal waveforms the displacement power factor is equal to  $\cos\varphi$ . Thus, in case of pure sinusoidal system, Displacement Power factor and True Power factor are equivalent.

In switching operative condition displacement power factor is established as

$$PF_{disp} = \frac{P_{avg}}{V_{in1,rms} \cdot I_{in1,rms}} \quad (18)$$

Where  $V_{in1,rms}$  and  $I_{in1,rms}$  are the first harmonic of the AC voltage and current respectively. The  $P_{avg}$  is defined as

$$P_{avg} = \sum_{i=1}^{\infty} V_{in(i),rms} \cdot I_{in(i),rms} \cdot \cos\varphi \quad (19)$$

Neglecting the Harmonic beyond the first one is valid the approximation of  $P_{avg1}$  related to the first harmonic quantities equal to  $P_{avg}$ , the true power factor can be established as the multiplication between the Distortion Power Factor and the Displacement Power Factor [48].

$$TPF = \frac{1}{\sqrt{1 + THD_i^2}} \cdot \frac{P_{avg1}}{V_{in1,rms} \cdot I_{in1,rms}} \quad (20)$$

In switching converter, to obtain a high TPF two target can be pursued: low  $THD_i$  and Displacement Power Factor very close to one. The control strategy target is to combine an input current quite close a sinusoidal waveform (high THD) with the same phase of the input voltage to reach high-PF. Furthermore, the common PFC control method is usually combined with a peak current control.

Indeed, several integrated control chips for Flyback converter are based on the peak current PFC control implementing also QR operation [49]. A basic function block diagram of the QR peak current mode IC is depicted in **Figure 15a**. In **Figure 15a**,  $V_{inr}$  is the rectified AC line voltage.  $V_{fb}$  is the signal feedback of the output voltage  $V_o$ .  $V_{ref}$  is the reference voltage. The output of the error amplifier 1 is a multiplier factor of a suitable reduced value of  $V_{inr}$  ( $k_p \cdot V_{inr}$ ). The bandwidth of the error amplifier is quite low to have in a slow variation of the output error (low pass filter effect) with a low ripple. The output of the multiplier block is proportional to  $V_{inr}$ . The signal voltage  $V_{Rs}$  is related to the primary inductor peak current. If  $V_{Rs}$  reaches the output voltage of the multiplier  $V_{Mu}$  the pulse width modulation (PWM) signal is reset turning off the power switch Q. The turn-on is achieved by the valley detect circuit (VDC) obtaining the waveforms depicted in **Figure 15b** The VDC acts after the full demagnetization of

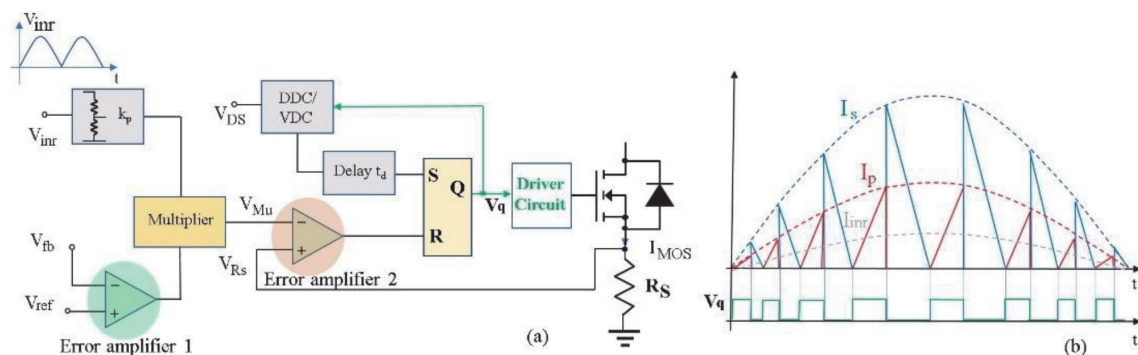


**Figure 15.**  
 (a) PFC control circuit simplified schematic. (b) Primary and secondary side current behavior and driver signal  $V_q$ .

the primary windings provided by an enable signal of a demagnetization detection circuit (DDC). The output signal of the VDC block set the delay time  $t_d$ . As shown in **Figure 15b** the current envelope both at the primary and secondary side is a half sinusoidal cycle. In particular, the inductor peak current will be a sine wave with the same phase as the input voltage, which can achieve a quite high-power factor. As above described, the control signal  $V_q$  has a non-constant frequency.

The controller can be used in the simple DCM operation without QR enhancement, replacing the VDC block with only the DDC and settling the delay time  $t_d$  at a constant value. In this last control approach, the driver signal  $V_q$  acts at constant frequency.

The control method investigation is based on the analysis detailed in [47, 50]. The control method quantities depending on the instantaneous line voltage. For simplicity of analysis in the following, the term  $\theta = 2\pi f_{line}t$  is considered. Where  $f_{line}$  is the frequency of the grid line quantities. Furthermore, the analysis is based on the following hypothesis.

- The input voltage  $V_{in}$  is fully sinusoidal.
- The coupling between the inductors on the Flyback is ideal.
- The power switch and the diodes have conduction and switching losses negligible).
- The output voltage is constant in a line half-cycle.
- The Flyback converter operates in DCM and QR with  $k = 1$

Based on the first assumption the voltage downstream the rectifier bridge is a rectified sinusoidal waveform.

$$V_{inr}(\theta) = V_{inr,pk} \cdot \sin \theta \quad (21)$$

Where  $V_{inr,peak}$  is the max peak amplitude of the rectified  $V_{inr}$ .

The current peak  $I_{p,pk}$  at the primary side is enveloped by a rectified sinusoid as shown in **Figure 15b**. It is given by. It is given by

$$I_{p,pk}(\theta) = I_{p,pk} \cdot \sin \theta \quad (22)$$

Where  $I_{p,pk}$  is the maximum peak amplitude of the enveloped current in the primary side. In the secondary side the  $I_{s,pk}$  is proportional to the primary current.

$$I_{s,pk}(\theta) = n \cdot I_{p,pk} \quad (23)$$

Where  $n$  is the transform ratio,  $n = N_p/N_s$ .

Considering the current  $I_p$  as a triangle form, as shown in **Figure 14b** and **c**,  $t_{on}$  is expressed by

$$t_{on} = \frac{L_M \cdot I_{p,pk}(\theta)}{V_{inr}(\theta)} \quad (24)$$

At turn-off,  $t_{off}$  is

$$t_{off} = \frac{L_s \cdot I_{s,pk}(\theta)}{V_0} = \frac{L_M \cdot I_{p,pk}(\theta)}{n \cdot V_0} \quad (25)$$

Considering the assumption of  $k = 1$  and neglecting the  $t_d$  for simplicity (very close to the CRM operation). The switching time  $T_{sw}$  is given by

$$T_{sw} = t_{on} + t_{off} = \frac{L_M \cdot I_{p,PK}}{V_{inr,pk}} \cdot \left[ 1 + \frac{V_{inr,pk}}{V_r} \cdot |\sin \theta| \right] \quad (26)$$

From (24) the minimum value of the stitching frequency  $f_{sw,min}$  is achieved at  $\sin \theta = 1$  (the peak of the rectified sinusoid).

$$f_{sw} = \frac{V_{inr,pk}}{L_M \cdot I_{p,PK}} \cdot \frac{1}{1 + \frac{V_{inr,peak}}{V_r}} \quad (27)$$

The duty cycle is given by

$$d(\theta) = \frac{t_{on}}{T_{SW}} = \frac{1}{1 + \frac{V_{inr,peak}}{V_r} \sin \theta} \quad (28)$$

The control strategy described above in **Figure 15b** leads to the envelope current on the primary stage following the sinusoid described by (22) and better specified as

$$I_{p,pk} = \frac{1}{L_M} \cdot (V_{inr,pk} \cdot \sin \theta) \cdot t_{on} \quad (29)$$

The rectified input current  $I_{inr}(\theta)$  can be established as the average value of the primary current in each triangle over a switching cycle (**Figure 15b**).

$$I_{inr}(\theta) = \frac{1}{2} \cdot I_{p,pk}(\theta) \cdot \frac{t_{on}(\theta)}{T_{sw}(\theta)} = \frac{1}{2L_M} (V_{inr,pk} \cdot \sin \theta) \cdot \frac{t_{on}^2(\theta)}{T_{sw}(\theta)} \quad (30)$$

The constraint design condition for achieve a displacement power factor equal to 1 is

$$d^2(\theta) \cdot T_{SW}(\theta) = \left[ \frac{t_{on}(\theta)}{T_{sw}(\theta)} \right]^2 \cdot T_{sw}(\theta) = \frac{t_{on}^2(\theta)}{T_{sw}(\theta)} = constant \quad (31)$$

### 4.3 Two-stage LED driver circuits

The two-stage driver converter is more expensive in terms of components used but offering better immunity to line disturbances and greater flexibility because the power factor control is separated by the DC-DC current allowing more simple dimmable applications. Furthermore, the modular The wide solution for the PFC topology is a boost converter. In power converters such as the Boost (also the SEPIC and Ćuk converter, but with more numerous components than the Boost) the switch non directly disconnect the power source (see **Figure 7**). This causes a not complete interruption of the input current such as in the Buck or Buck-Boost topologies. Furthermore, the current ripple can be smoothly controlled from the converter, making the Boost topology very attractive for active PFC. To increase the power rate requested an interleaved solution can be adopted [51].

The second stage DC-DC converter topology depends on the power rate requested. Over the 100 W Half and Full Bridge topologies are implemented as described in **Figure 12**. Usually, an isolated resonant converter is considered to increase the efficiency and reduce the EMI contents. In the resonant topologies, the

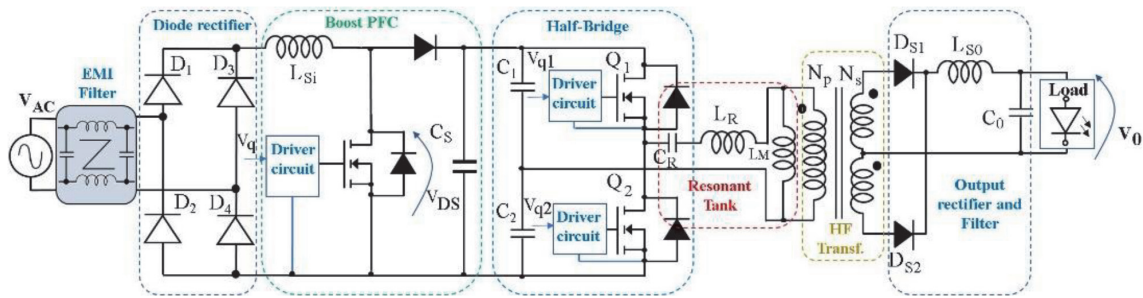


**Figure 16.**

Two stage LED driver circuit composed by PFC boost converter and half-bridge LLC converter.

LLC converter is mainly adopted in LED driver applications because of its soft-switching characteristic. The LLC converter features zero-voltage switching turn-on of the switches on the primary side and zero-current turn-off for the rectifier diodes on the secondary side. The soft-switching transients allow both low noises and reduced stress during the switches transients. In addition, the LLC converter regulates the output voltage in a wide-output voltage. Moreover, the isolated high-frequency transformer allows a multi-output driver circuit for the string LEDs solution. In **Figure 16** two stage LED driver composed by a Boost PFC converter and Half-Bridge LLC converter useful for load until 500 W is reported.

#### 4.4 Boost PFC circuit evaluation

The Boost PFC converter has a simple topology. The switch driver circuit is referenced to the ground reducing the driver switching noises. Furthermore, it can guarantee a power factor close to one obtainable with several control techniques [52]. It allows an input current with low distortion and an output voltage with a very low ripple thanks to the presence of the capacitor  $C_s$ . On the other hand, the presence of the capacitor  $C_s$  produces high currents during converter switching on and has an intrinsic weakness in the short circuit as the output is connected directly to the input by means of the inductor  $L_s$ . At higher powers, it needs to run on CCM to ensure adequate power transfer. In this operation mode, the current in the inductor never reaches zero during the switching cycle. Usually, the most used controllers for these applications are based on the average current control that allows CCM operation. The Boost PFC scheme with the average current control is described in **Figure 17**.

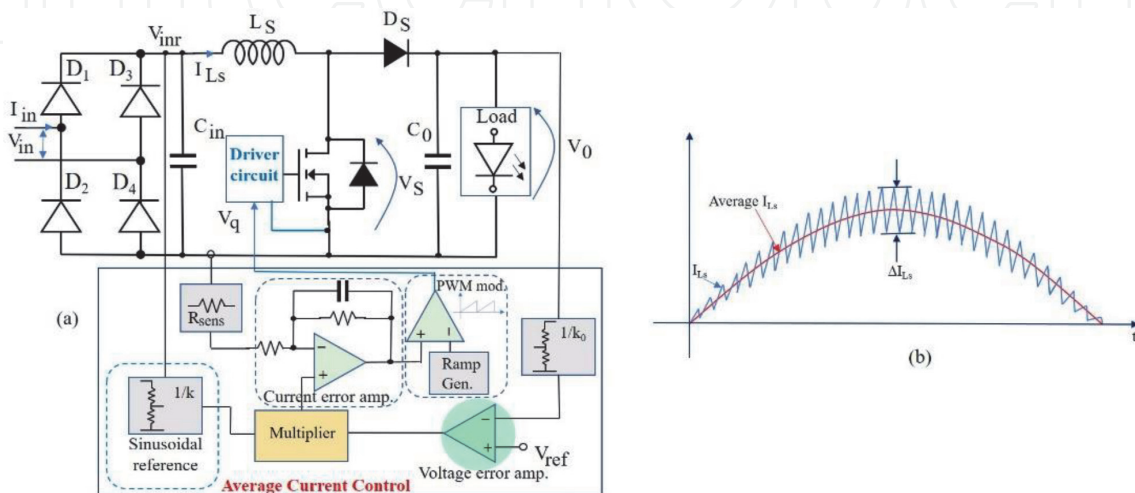


**Figure 17.**

(a) Simplified block scheme of the boost PFC with average current control. (b) Inductor average and ripple currents.

The control loop to obtain the average current mode maintains the current proportional to the input voltage. While the voltage control loop regulates the output voltage to the boost value requested.

The advantages of the average current control are the following

- a constant switching frequency;
- little sensitivity to switching noises;
- the high quality of input current waveforms with reduced inductor current ripple
- the maximum peak current in the switching device is reduced

The disadvantages concern

- the need to sense the current in the inductor;
- the need to insert a compensation network in the current amplifier which takes into account the characteristics of the converter used and the duty point during the line voltage cycle.

In **Figure 17b** the inductor average current behavior and the inductor current ripple are shown. The value of  $\Delta I_{Ls}$  is chosen during the design phase in the range from 20 to 25% of the peak of the input current  $I_{in}$ . The input peak current in the case of pure sinusoidal waveform is given by

$$I_{in,pk} = \frac{\sqrt{2} \cdot P_{in,max}}{V_{in,rms,min}} \quad (32)$$

Where  $P_{in,max}$  is the input power at the maximum output power requested. It is given by

$$P_{in,max} = \frac{P_{0,max}}{\eta_{min}} \quad (33)$$

With  $\eta_{min}$  is the minimum converter efficiency.  
 The peak inductor current is

$$I_{Ls,pk} = I_{in,pk} + \frac{\Delta I_{Ls}}{2} \quad (34)$$

Where

$$\Delta I_{Ls} = K_{\Delta I} \cdot I_{in,pk} \quad (35)$$

Where  $K_{\Delta I}$  is the inductor ripple factor (supposing 20% of the  $\Delta I_L$  maximum,  $K_{\Delta I} = 0.20$ ). To design the Boost inductance, the duty cycle at the peak of the minimum sinusoidal input voltage is considered. The value of the rectified voltage is obtained from

$$V_{in,pk,min} = \sqrt{2} \cdot V_{in,pk,min}(\theta) \quad (36)$$

The duty cycle at the minimum input voltage and considering the required output voltage (approximately it is a constant voltage) is calculated by

$$d = \frac{V_0 - V_{in,pk,min}}{V_0} \quad (37)$$

then, the inductance  $L_s$  is given by

$$L_s = \frac{V_{in,pk,min} \cdot d}{f_{sw} \cdot \Delta I_{L_s}} \quad (38)$$

The purpose of the output capacitor  $C_{in}$  in **Figure 17a** is to filter the high-frequency current component of the inductance.

The HF capacitor acts as an EMI filter minimizing the HF harmonic component (this HF current component are shorted by  $C_{in}$ ) [53].

The HF capacitor design is a trade-off to minimize the noise injected into the line grid and the value that avoid zero-crossing line current distortion.  $C_{in}$  is given by

$$C_{in} = K_{\Delta I} \cdot \frac{I_{in,pk}}{2\pi \cdot f_{sw} \cdot r \cdot V_{in,pk,min}} \quad (39)$$

Where  $K_{\Delta I} = 0.20$  and  $r$  is input voltage ripple factor ( $\Delta V_{in}/V_{in}$ ) settled usually in the range of 5–6%. An HF film capacitor with low ESL and high-voltage rating (630 V for European line voltage of 230 V). Usually, ceramic technology capacitor is selected for this converter application.

The output capacitor selection  $C_0$  is related to the output voltage maximum ripple required ( $\Delta V_0$ ).  $C_0$  is calculated by

$$C_0 \geq \frac{P_0}{2\pi \cdot f_{sw} \Delta V_0 \cdot V_0} \quad (40)$$

As the required power increases ( $\geq 500$  W), the PFC converter performances can be optimized by adopting an interleaved solution. The interleaved Boost topology is obtained connecting two or more single Boost legs as shown in **Figure 18**, controlling the switching of every MOSFET with a proper control strategy.

The command signals of the switches are supplied in out of phase mode according to

$$phaseshift = \frac{360^\circ}{N_c} \quad (41)$$

where  $N_c$  is the number of legs in the interleaved boost circuit. Despite the increase in the number of components and a more complex control technique, in the interleaved topologies several advantages are shown.

- Reduced overall input current ripple.
- Reduced electromagnetic contents and consequently EMI filter.
- Reduction of the magnetics components size.
- RMS current rating decrease in the output capacitance.

- Use of the power semiconductor devices with a less current rate.
- Reduction of conduction diode and MOSFET losses thanks to the parallel structure.

In the interleaved topology the reduced current ripple allows to avoid the capacitor  $C_{in}$ . A complete design of 3 kW PFC based on an interleaved PFC Boost converter is reported in [54]. The control technique is based on Microcontroller Units (MCUs) or specialized Integrated Circuits (ICs). An example of the high-performance IC controller of common use is the FAN9673 (On-Semiconductor) [55]. It is an interleaved three-channel CCM PFC controller, implementing a channel management function. It enables a single cell at light load (less than one-third of the rated load) or two or three cells depending on power – level request. The interleaved cells management optimizes PFC efficiency. Three legs interleaved Boost PFC schematic linked to the line grid by a diode rectifier bridge and EMI filter is shown in **Figure 18**.

#### 4.5 Half-bridge LLC converter notes

LLC resonant converter in its half-bridge implementation is more popular in LED driver circuit for the low switching noise and the capability to achieve a high-power density. An HF transformer is used to attain galvanic isolation. A compact volume is obtained by integrating part of the resonant tank into the HF transformer sizing. In this design approach, the transformer arrangement leads to satisfying the requirements on  $L_M$  and  $L_R$ , thus avoiding adding additional external components. Thus, the transformer inductive parameters and a series-connected capacitor  $C_R$  are used to make a resonant tank. The LLC solution allows Buck and Boost transfer characteristics in the soft-switching operative region. The switching devices  $Q_1$  and  $Q_2$  operate at a duty cycle of just under 50% to avoid cross conduction. The output voltage is regulated through a variation of the converter switching frequency. The converter features two resonant frequencies. The resonant frequency depends of the resonant tank components and the load conditions. The higher resonant

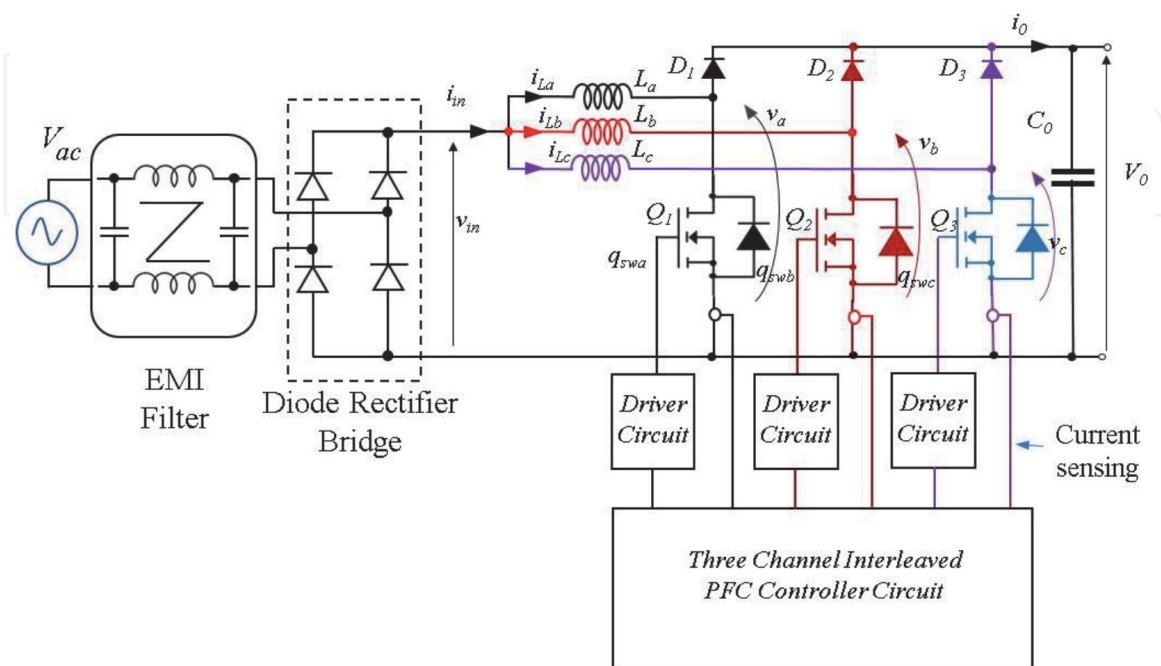


**Figure 18.**  
 Three channel boost PFC simplified electrical scheme.



frequency  $f_{r1}$  occurs considering the higher load conditions. In this case the  $L_M$  can be neglected and  $f_{r1}$  is given by

$$f_{r1} = \frac{1}{2\pi \cdot \sqrt{L_R \cdot C_R}} \quad (42)$$

A lower resonant frequency  $f_{r2}$  appears at light load operation. In this operative condition,  $L_M$  must be considered. The resonant frequency consequently changes.

$$f_{r2} = \frac{1}{2\pi \cdot \sqrt{(L_R + L_M) \cdot C_R}} \quad (43)$$

From (42) and (43) appears that  $f_{r1} > f_{r2}$ . The frequency  $f_{r2}$  is also called the second resonance frequency. The LLC converter can operate in several ways related to the input voltage and load current conditions. The difference between the two resonant frequencies depends on the relationship between  $L_M$  and  $L_R$ . Usually, the LLC converter operates at a constant duty cycle. The condition  $f_{sw} < f_{r2}$  is not used in actual applications because an instability condition arises from the study of the transfer function of the converter [56]. In LLC converter there are three different operative conditions:  $f_{r2} > f_{sw} > f_{r1}$ ,  $f_{sw} = f_{r1}$  and,  $f_{sw} > f_{r1}$ . Referring to the LLC converter shown in **Figure 19a**, the resonant converter waveforms in the three operation modes are shown in **Figure 19b**.

At resonant frequency operation, at  $f_{sw} = f_{r1}$ , the resonant tank has unity gain and the best efficiency is reached. Primary-side and secondary-side RMS currents are the lowest values. In the primary-side switches, ZVS operation is achieved while on the secondary-side the diodes operate in zero current switching (ZCS). Furthermore, in the narrow neighborhood of  $f_{r1}$  the gain does not depend on the load conditions [57]. The analysis of the gain behavior depending on the electrical parameters of the resonant tank and load request. A detailed analysis is reported in [58].

At the  $f_{sw}$  above  $f_{r1}$ , the switching period is shorter than the resonant period. The resonant half cycle is not fully completed by the starting of the other half of the switching cycle, as shown in **Figure 19b**. In this case, on the secondary side, the rectifier diodes do not achieve the ZCS operating in hard switching. Also in this

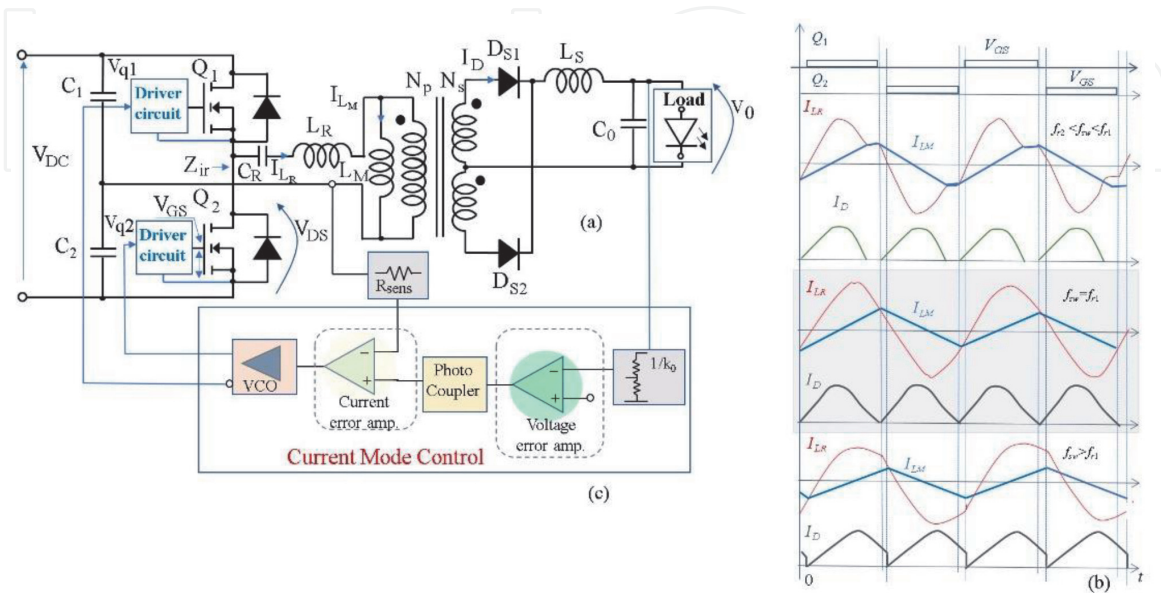


**Figure 19.**

(a) LLC converter schematic. (b) Main converter waveforms at  $f_{r2} > f_{sw} > f_{r1}$ ,  $f_{sw} = f_{r1}$  and,  $f_{sw} > f_{r1}$ . (c) Simplified current mode controller with VCO.

operative condition, on the primary-side switches, the ZVS is reached. Finally, the resonant tank features a voltage gain lower than unity.

In the switching frequency between the two resonant frequencies ( $f_{r2} > f_{sw} > f_{r1}$ ). The resonant tank gives a voltage gain higher than unity. The primary-side switches commute in ZVS and in the secondary-side diodes achieve ZCS. In this operative condition, the peak value of the resonant current circulating through the  $L_M$  is larger leading to higher conduction losses through the converter. Based on the load the equivalent impedance connected to the half-bridge switching leg can be either inductive or capacitive at frequency variation. Usually, the LLC converter operates in the region where the input impedance of the resonant tank has an inductive behavior (i.e. it increases with  $f_{sw}$ ) [59]. Furthermore, the ZVS mode on the primary-side is achieved only if the tank input impedance  $Z_{ir}$  is inductive. This operative condition can be controlled by changing the switching frequency. Higher output power is obtained by reducing the frequency and vice versa.

In the LED driver application, the output current must be controlled. In LLC the current mode controller is arranged with a voltage-controlled oscillator (VCO) that change the current control signal in variable switching frequency to drive the primary-side MOSFETs [60]. A simplified schematic of the current control with the VCO block is depicted in **Figure 19c**. The drawback of the LLC converter results from the difficulty in achieving consistent dynamic performance over wide-operating conditions. To reduce the switching losses on the secondary-side a synchronous rectifier solution may be arranged. In this case the diodes are replaced by low voltage MOSFETs driven in synchronous mode by a suitable control technique [61].

#### 4.6 Multiple outputs LED driver circuits

Multi-channel LED structure is popularly implemented in some lighting systems such as indoor lighting and street lighting. Also, in display backlighting, advanced color-mixing and dimming LED systems the multi-channel LED driver solutions are used [62]. The multi-channel LED topologies connected to the line grid are usually composed of traditional five stages: the EMI filter, the bridge rectifier PFC stage, front-end DC/DC stage and multi-channel post-current-regulator stage. In multiple outputs LED driver independent output current control can be necessary. The post-current regulator can be performed in a linear mode current regulator or switch-mode converter.

A simplified block schematic of the multi-channel constant current LED driver is reported in **Figure 20a**.

In the isolated LED driver solutions, the Flyback converter is widely used in multiple-output Flyback LED driver to integrate DC-DC converter with PFC circuit. The constant current source of multiple channel LED can be supplied in linear mode as shown in **Figure 20b** or with switch-mode converter as depicted in **Figure 20c** [63]. In **Figure 20c** the current source for the LED string is achieved by a synchronous Buck current regulator to reduce the power losses.

In multi-channel applications there are also non-isolated LED driver circuits application. In this kind of LED driver, the single-inductor multiple-output (SIMO) structure is more attractive [64]. It is based on several Buck converters arrangement. In the SIMO solution LED strings current are regulated by switching Buck-type power converters. Furthermore, a main Buck converter is used to interface the rectified voltage performing the PFC functions [65]. The inductor of the main Buck converter is shared with the multi-channel Buck regulators. The simplified schematic of the SIMO structure is shown in **Figure 21**. The noticeable advantage of the SIMO technologies is their compact size the low cost and high-power efficiency especially at the increasing of LED strings.

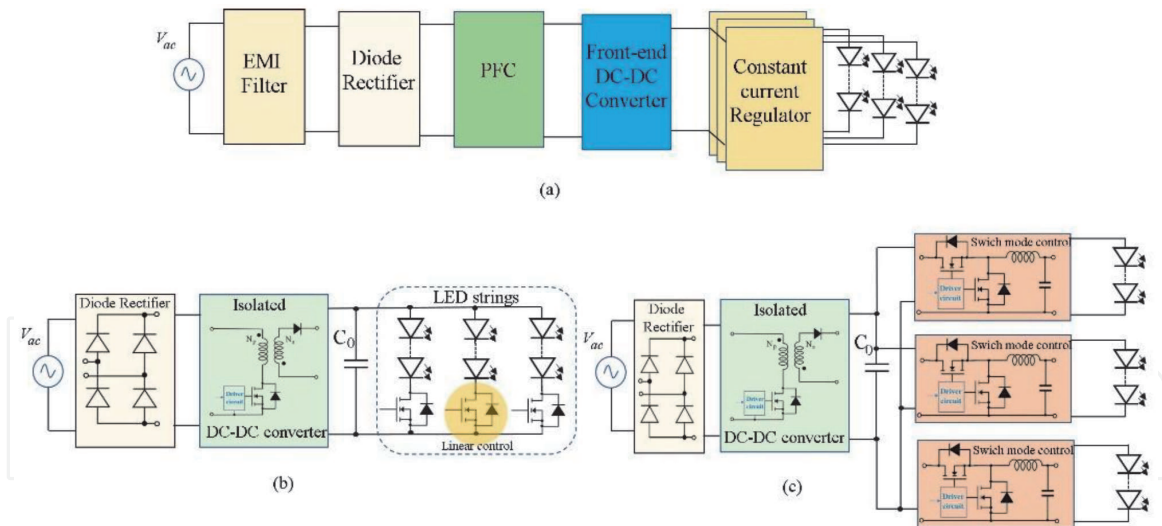


**Figure 20.**

Multi-channel LED driver circuits (a) block scheme of general AC LED driver system for multi-channel LED string. (b) Flyback converter solution with linear regulator on the secondary side. (c) Flyback converter solution with switching type synchronous Buck current regulator.

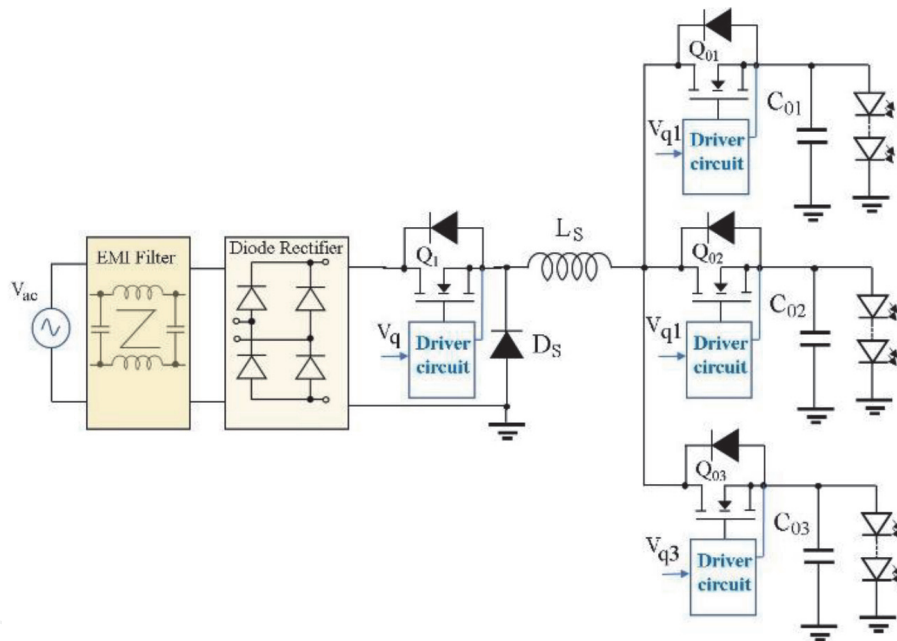


**Figure 21.**

Multi-channel LED driver circuits with single-inductor multiple-output solution.

For high current LED string the LLC converter with multiple-output secondary of the HF transformer can be considered [66]. In the secondary side as described in **Figure 20b** and **Figure 20c** a switching or linear type current regulator is added to drive the LED strings.

## 5. Conclusion

The LED driver circuits in several applications needs are investigated. The passive and active circuits are critically evaluated in terms of power request, topology simplicity, efficiency, reliability, and cost. The LED driver circuits are evaluated based on the different supply sources and power request. The DC-DC converters connected directly to a DC source such as battery are classified and pro and cons are

discussed. The main current control strategies are described, and the dimming features are also considered. Furthermore, the power converters connected to the AC line are explored considering the one-stage and two-stage converter solutions. In the one-stage LED driver a Flyback converter description is focused. The design issues and the control method to meet the output current regulation and the high-power factor request are explored. Afterwards, the two-stage driver converters for higher power applications are investigated. The first stage Boost converter PFC circuit design and control issues are examined, and the interleaved solution is introduced. The second stage LLC for a higher current LED driver is also considered providing basic information on the operation and the applications. Finally, multi-channel LED driver circuits in non-isolated and isolated conditions are presented and discussed.

IntechOpen

### **Author details**


Salvatore Musumeci

Department of Energy “G. Ferraris”, Politecnico di Torino, Torino, Italy

\*Address all correspondence to: [salvatore.musumeci@polito.it](mailto:salvatore.musumeci@polito.it)

### **IntechOpen**

---

© 2021 The Author(s). Licensee IntechOpen. This chapter is distributed under the terms of the Creative Commons Attribution License (<http://creativecommons.org/licenses/by/3.0>), which permits unrestricted use, distribution, and reproduction in any medium, provided the original work is properly cited. 

## References

- [1] Wang Y Y, Alonso J M, Ruan X. A Review of LED Drivers and Related Technologies. *IEEE Transactions on Industrial Electronics*. 2017; 64 (7): 5754–5765. Doi: 10.1109/TIE.2017.2677335.
- [2] Zissig G, Bertoldi P. Status of LED-Lighting world market in 2017. European commission, JRC Technical Report, [Internet] 2018. Available from: <https://e3p.jrc.ec.europa.eu/publications/status-led-lighting-world-market-2017>
- [3] Arias M, Vázquez A, Sebastián J. An Overview of the AC-DC and DC-DC Converters for LED Lighting Applications. *Automatika*. 2012; 53 (2): 156–172. DOI: 10.7305/automatika.53-2.154.
- [4] Di Mauro S, Musumeci S, Raciti A. Analysis of electrical and photometric quantities of CFL and LED bulb lamp. In: *Proceedings of the IEEE Industry Applications Society Annual Meeting (IAS '17)*; 1–5 Oct. 2017; Cincinnati OH: IEEE; 2017. p. 1–8.
- [5] Di Mauro S, Raciti A, Rizzo S A, Susinni G, Musumeci S. Effects of the aging time on CFL and LED lamps: experimental tests on the electrical and photometric quantities. In: *Proceedings of the AEIT International Annual Conference (AEIT '18)*; 3–5 Oct. 2018; Bari. Italy: IEEE; 2018. p. 1–6.
- [6] Uddin S, Shareef H, Mohamed A, Hannan M A, Mohamed K. LEDs as energy efficient lighting systems: A detail review. In: *Proceedings of the IEEE Student Conference on Research and Development*, 19–20 Dec. 2011; Cyberjaya. Malaysia: IEEE; 2011 p. 468–472.
- [7] Ogunjuyigbe A S O, Ayodele T R, Idika V E, Ojo O. Effect of lamp technologies on the power quality of electrical distribution network. In: *Proceedings of the IEEE PES PowerAfrica*, 27–30 June 2017; Accra. Ghana: IEEE; 2017. p. 159–163.
- [8] Life-Cycle Assessment of Energy and Environmental Impacts of LED Lighting Products Part I: Review of the Life-Cycle Energy Consumption of Incandescent, Compact Fluorescent, and LED Lamps February 2012, Updated August 2012. [Internet]. 2012 Available from: [https://www1.eere.energy.gov/buildings/publications/pdfs/ssl/2012\\_LED\\_Lifecycle\\_Report.pdf](https://www1.eere.energy.gov/buildings/publications/pdfs/ssl/2012_LED_Lifecycle_Report.pdf).
- [9] Görbe P, Magyar A, Csuti P. Power Quality Management of LED Light Sources in Frequency Domain. *Chemical Engineering Transactions*, 2013; 35: 1309–1314. <https://doi.org/10.3303/CET1335218>
- [10] Di Mauro S, Raciti A, Rizzo S A, Susinni G, Musumeci S. Steady-state equivalent circuit of LED bulbs accounting for the current harmonics. In: *Proceedings of the IEEE 44th Annual Conference of the IEEE Industrial Electronics Society (IECON '18)*, 21–23 Oct. 2018; Washington DC. USA: IEEE; 2018. p. 1513–1518.
- [11] Luz P C V, Bolzan P E, Kirsten A L, do Prado R N. Isolated topologies family for street lighting using LED as source light. In: *Proceedings of the IEEE 42nd Annual Conference of the IEEE Industrial Electronics Society (IECON '16)*; 10–16 Oct. 2016; Florence. Italy: IEEE; 2016. p. 3451–3457.
- [12] Adam GK. DALI LED Driver Control System for Lighting Operations Based on Raspberry Pi and Kernel Modules. *Electronics*. 2019; 8(9):1021. <https://doi.org/10.3390/electronics8091021>.
- [13] Lehman B, Wilkins A J. Designing to Mitigate Effects of Flicker in LED Lighting: Reducing risks to health and

- safety. *IEEE Power Electronics Magazine*. 2014; 1 (3): 18–26. Doi: 10.1109/MPEL.2014.2330442.
- [14] Castro I, Vazquez A, Arias M, Lamar D G, Hernando M M, Sebastian J. A Review on Flicker-Free AC–DC LED Drivers for Single-Phase and Three-Phase AC Power Grids. *IEEE Transactions on Power Electronics*. 2019; 34 (10): 10035–10057. Doi: 10.1109/TPEL.2018.2890716.
- [15] Li S, Tan S, Lee C K, Waffenschmidt E, Hui S Y, Tse C K. "A survey, classification, and critical review of light-emitting diode drivers," *IEEE Transactions on Power Electronics*. 2016; 31 (2): 1503–1516. Doi: 10.1109/TPEL.2015.2417563.
- [16] Direct-AC, Linear LED Driver Topology: CCR Straight Circuit (120 VAC & 230 VAC). Design Note – DN05079/D. On-Semiconductor [Internet]. 2015. Available from <https://www.onsemi.com/pub/Collateral/DN05079-D.PDF>
- [17] Chen W, Li S N, Hui S Y R. A comparative study on the circuit topologies for offline passive light-emitting diode (LED) drivers with long lifetime & high efficiency. In *Proceedings of IEEE Energy Conversion Congress and Exposition (ECCE '10)*; 12–16 Sept. 2010; Atlanta, GA, USA: IEEE; 2010. p. 724–730.
- [18] Tung NT, Tuyen ND, Huy NM, Phong NH, Cuong NC, Phuong LM. Design and Implementation of 150 W AC/DC LED Driver with Unity Power Factor, Low THD, and Dimming Capability. *Electronics*. 2020; 9(1):52. <https://doi.org/10.3390/electronics9010052>
- [19] Li S, Tan S, Lee C K, Waffenschmidt E, Hui S Y, Tse C K. A survey, classification, and critical review of light-emitting diode drivers. *IEEE Transactions on Power Electronics*. 2016; 31 (2): 1503–1516. Doi: 10.1109/TPEL.2015.2417563.
- [20] Hui S Y, Li S N, Tao X H, Chen W, Ng W M. A Novel Passive Offline LED Driver with Long Lifetime. *IEEE Transactions on Power Electronics*. 2010; 25 (10): 2665–2672. Doi: 10.1109/TPEL.2010.2048436.
- [21] Cosp-Vilella J, Martínez-García H. Design of an on-chip linear-assisted DC-DC voltage regulator. In: *Proceedings of the IEEE 20th International Conference on Electronics, Circuits, and Systems (ICECS '13)*; Abu Dhabi. United Arab Emirates: IEEE; 2013. p. 353–356.
- [22] NUD4001, ON-Semiconductor, Datasheet [Internet]. 2011. Available from: <https://www.onsemi.com/pub/Collateral/NUD4001-D.PDF>
- [23] Chiu H, Lo Y, Chen J, Cheng S, Lin C, Mou S. A High-Efficiency Dimmable LED Driver for Low-Power Lighting Applications. *IEEE Transactions on Industrial Electronics*. 2010; 57 (2): 735–743. Doi: 10.1109/TIE.2009.2027251.
- [24] Hurley W G, Wolfle W H, Breslin J G. Optimized transformer design: inclusive of high-frequency effects. *IEEE Transactions on Power Electronics*. 1998; 13 (4): 651–659. Doi: 10.1109/63.704133.
- [25] Doshi M, Zane R. Digital Architecture for Driving Large LED Arrays with Dynamic Bus Voltage Regulation and Phase Shifted PWM. In: *Proceedings of the IEEE Twenty-Second Annual Applied Power Electronics Conference and Exposition, (APEC '07)*; 25 Feb.-1 March 2007; Anaheim CA. USA: IEEE; 2007. p. 287–293.
- [26] Lin W, Chen H, Ke S. Research on a single-stage Flyback/boost LED driver with lower output ripple. In: *Proceedings of the IEEE 2nd Annual*

- Southern Power Electronics Conference (SPEC '16); 5–8 Dec. 2016; Auckland. New Zealand: IEEE; 2016. p. 1–5.
- [27] Qiu Y, Wang L, Wang H, Liu Y, Sen P C. Bipolar Ripple Cancellation Method to Achieve Single-Stage Electrolytic-Capacitor-Less High-Power LED Driver. *IEEE Journal of Emerging and Selected Topics in Power Electronics*. 2015; 3 (3): 698–713. Doi: 10.1109/JESTPE.2015.2433918.
- [28] Athalye P, Harris M, Negley G. A two-stage LED driver for high-performance high-voltage LED fixtures. In: *Proceedings of the IEEE Twenty-Seventh Annual IEEE Applied Power Electronics Conference and Exposition (APEC '12)*; 5–9 Feb. 2012; Orlando. FL. USA: IEEE; 2012. p. 2385–2391.
- [29] Castro I, Lamar D G, Arias M, Hernando M M, Sebastian J. Multicell Three-Phase AC–DC Driver for HB-LED Lighting Applications. *IEEE Transactions on Industry Applications*. 2017; 53 (4): 3803–3813. Doi: 10.1109/TIA.2017.2686802.
- [30] Chen W, Cheng KWE, Shao J. Circuit Topology Analysis for LED Lighting and its Formulation Development. *Energies*. 2019; 12(21):4203. <https://doi.org/10.3390/en12214203>.
- [31] Ferdous S M, Oninda M A M, Sarowar G, Islam K K, Hoque M A. Non-isolated single stage PFC based LED driver with THD minimization using Cúk converter. In: *Proceedings of the IEEE 9th International Conference on Electrical and Computer Engineering (ICECE '16)*; 20–22 Dec. 2016; Dhaka. Bangladesh: IEEE; 2016. p. 471–474.
- [32] Jha A, Singh B. SEPIC PFC converter fed LED driver. In: *Proceedings of the IEEE 1st International Conference on Power Electronics, Intelligent Control and Energy Systems (ICPEICES '16)*, Delhi. India: IEEE 2016. p. 1–6.
- [33] In-Hwan Oh. An analysis of current accuracies in peak and hysteretic current controlled power LED drivers. In: *Proceedings of the IEEE Twenty-Third Annual IEEE Applied Power Electronics Conference and Exposition (APEC '08)*; 24–28 Feb. 2008; Austin. TX. USA: IEEE; 2008 p. 572–577.
- [34] Shao J. Single Stage Offline LED Driver. In: *Proceedings of the IEEE Twenty-Fourth Annual IEEE Applied Power Electronics Conference and Exposition (APEC '09)*; 15–19 Feb. 2009; Washington. DC. USA: IEEE; 2009. p. 582–586.
- [35] Deng H, Shan L, Yin Y, Si G, Sun Y. Design of a LED constant-current driver using a novel hysteresis-current control method with adaptive off-time control. In: *Proceedings of the IEEE 8th International Congress on Image and Signal Processing (CISP '15)*; 14–16 Oct. 2015; Shenyang. China: IEEE; 2015. p. 1551–1555.
- [36] Faraci E, Seeman M, Gu B, Ramadass Y, Brohlin P. High efficiency and power density GaN-based LED driver. In: *Proceedings of the IEEE Applied Power Electronics Conference and Exposition (APEC '16)*; 20–24 March 2016; Long Beach. CA. USA: IEEE; 2016. p. 838–842.
- [37] Puukko J, Xu J; Liu L. Consideration of flyback converter using GaN devices. In: *Proceedings of the IEEE 3rd Workshop on Wide Bandgap Power Devices and Applications (WiPDA '15)*; 2–4 Nov. 2015; Blacksburg. VA. USA: IEEE; 2015. p. 196–200.
- [38] Zhang X, Liu H, Xu D. Analysis and design of the flyback transformer. In: *Proceedings of the IEEE 29th Annual Conference of the IEEE Industrial Electronics Society (IECON'03)*; 2–6 Nov. 2003; Roanoke. VA. USA: IEEE; 2003. p. 715–719.
- [39] Wang X, Tang J, Zhang X, Xie S, Mao X, Chen H. A High-Efficiency High

- Power Driver Circuit for Joint Illumination and Communication System With Phase Shift Pre-Emphasis Technology. *IEEE Access*. 2020; 9: 6325–6333. Doi: 10.1109/ACCESS.2020.3048168.
- [40] Zeng J, Zhang G, Yu S S, Zhang B, Zhang Y. LLC resonant converter topologies and industrial applications — A review. *Chinese Journal of Electrical Engineering*. 2020; 6 (3): 73–84. Doi: 10.23919/CJEE.2020.000021.
- [41] ENERGY STAR Program Requirements for Solid State Lighting Luminaires, Eligibility Criteria - Version 1.1. [Internet]. 2008. Available from: [http://www.energystar.gov/index.cfm?c=new\\_specs.ssl\\_luminaires](http://www.energystar.gov/index.cfm?c=new_specs.ssl_luminaires)
- [42] Gritti G, Adragna C. Primary-controlled constant current LED driver with extremely low THD and optimized phase-cut dimming compatibility. In: *Proceedings of the IEEE 17th European Conference on Power Electronics and Applications (EPE'15 ECCE-Europe)*; 8–10 Sept. 2015; Geneva. Switzerland: IEEE; 2015. p. 1–10.
- [43] Hu Y, Huber L, Jovanovic M M. Single-Stage Flyback Power-Factor-Correction Front-End for HB LED Application. In: *Proceedings of the IEEE Industry Applications Society Annual Meeting (IAS '09)*; 4–8 Oct. 2009; Houston. TX. USA: IEEE; 2009. p. 1–8.
- [44] Al-Naemi F, Yang J, Zhang W. A Low Power Single-stage LED Driver Operating between Discontinuous Conduction Mode and Critical Conduction Mode. *Elsevier, Energy Procedia*. 2015; 74: 817–825. <https://doi.org/10.1016/j.egypro.2015.07.817>.
- [45] Xu Y, Lin J, Xie X, Cai C. Design of a single-stage Flyback LED Constant current Driving Power Supply. *Journal of Physics: Conference Series, IOP Publishing*. 2019; 1288; 012086: 1–7. Doi: 10.1088/1742-6596/1288/1/012086.
- [46] Wu S. Single-Stage High Power Factor Flyback for LED Lighting. Richtek, Application Note, AN012 [Internet]. 2014. Available from: <https://www.richtek.com/Design%20Support/Technical%20Document/AN012>
- [47] Adragna C, Gritti G, Raciti A, Rizzo SA, Susinni G. Analysis of the Input Current Distortion and Guidelines for Designing High Power Factor Quasi-Resonant Flyback LED Drivers. *Energies*. 2020; 13(11):2989. <https://doi.org/10.3390/en13112989>.
- [48] Mack Grady W, Gilleskie R J. Harmonics and How they Relate to Power Factor. In: *Proceedings of the EPRI Power Quality Issues & Opportunities Conference (PQA'93)*; November 1993; San Diego. CA. pp 1–8.
- [49] Adragna C, Gritti G. High-power-factor quasi-resonant flyback converters draw sinusoidal input current. In: *Proceedings of the IEEE Applied Power Electronics Conference and Exposition (APEC '15)*; 15–19 March 2015; Charlotte. NC. USA: IEEE; 2015. p. 498–505.
- [50] Gritti G, Adragna C. Analysis, design and performance evaluation of an LED driver with unity power factor and constant-current primary sensing regulation. *AIMS Energy*. 2019; 7 (5): 579–599. Doi: 10.3934/energy.2019.5.579.
- [51] Cheng C, Cheng H, Chang C, Yang F, Chung T. A single-stage LED driver for street-lighting applications with interleaving PFC feature. In: *Proceedings of the IEEE International Symposium on Next-Generation Electronics (ISNE '13)*; 25–26 Feb. 2013; Kaohsiung. Taiwan: IEEE; 2013. p. 150–152.
- [52] Rossetto L, Spiazzi G, Tenti P. Control Techniques for Power Factor Correction Converters. In: *Proceedings of the International Conference on*



Power Electronics and Motion Control, September 1994; Warsaw. Poland. p. 1310-1318.

[53] Narahariseti K, Green P B. Design of 200 W boost PFC plus HB LLC resonant converter with IR1155, IRS27952 and IR11688. Infineon Application Note, AN1907 PL88 1908 004522 [Internet]. 2020. Available from: [https://www.infineon.com/dgdl/Infineon-LLC\\_Resonant\\_Converter\\_IR1155\\_IRS27952\\_IR11688-ApplicationNotes-v02\\_02-EN.pdf?fileId=5546d4626cb27db2016d003926ff1da3](https://www.infineon.com/dgdl/Infineon-LLC_Resonant_Converter_IR1155_IRS27952_IR11688-ApplicationNotes-v02_02-EN.pdf?fileId=5546d4626cb27db2016d003926ff1da3).

[54] Musumeci S, Bojoi R, Armando E, Borlo S, Mandrile F. Three-Legs Interleaved Boost Power Factor Corrector for High-Power LED Lighting Application. *Energies*. 2020; 13(7):1728. <https://doi.org/10.3390/en13071728>.

[55] Musumeci S, Bojoi R, Borlo S, Armando E. IGBT based Three Channel Interleaved PFC Boost Converter for Inverter Front-End Application. In: *Proceedings of the IEEE AEIT International Annual Conference (AEIT 2019)*; 18–20 Sept. 2019; Florence. Italy: IEEE; 2019. p. 1–6.

[56] Musumeci S. Inductor Constraints on LLC Converter Design in Battery Charger Applications. In: *Proceedings of the IEEE 5th International Forum on Research and Technology for Society and Industry (RTSI '19)*; 9–12 Sept. 2019; Florence. Italy: IEEE; 2019. p. 269–274.

[57] Musumeci S, Cristaldi D, Portoghese F. Super-junction power MOSFET in half bridge DC-DC zero-voltage converter for energy conversion management. In: *Proceedings of the IEEE International Conference on Clean Electrical Power (ICCEP '15)*; 16–18 June 2015; Taormina. Italy: IEEE; 2015. p. 755–760.

[58] De Simone S, Adragna C, Spini C, Gattavari G. Design-oriented steady-

state analysis of LLC resonant converters based on FHA. In: *Proceedings of the IEEE International Symposium on Power Electronics, Electrical Drives, Automation and Motion (SPEEDAM '06)*; 23–26 May 2006; Taormina. Italy: IEEE; 2006. p. 200–207.

[59] Han J-H, Lim Y-C. Design of an LLC Resonant Converter for Driving Multiple LED Lights Using Current Balancing of Capacitor and Transformer. *Energies*. 2015; 8(3):2125–2144. <https://doi.org/10.3390/en8032125>.

[60] Jang J, Pidaparthi SK, Choi B. Current Mode Control for LLC Series Resonant DC-to-DC Converters. *Energies*. 2015; 8(6):6098–6113. <https://doi.org/10.3390/en8066098>.

[61] Di Mauro S, Musumeci S, Raciti A, Fusillo F, Scrimizzi F, Scollo R. Synchronous rectification with low voltage MOSFETs in LLC converters. In: *Proceedings of the IEEE AEIT International Annual Conference (AEIT '17)*; 20–22 Sept. 2017; Cagliari. Italy: IEEE; 2017. p. 1–6.

[62] Wu H, Ji S, Lee F C, Wu X. Multi-channel constant current (MC3) LLC resonant LED driver. In: *Proceedings of the IEEE Energy Conversion Congress and Exposition, Phoenix (ECCE '11)*; 17–22 Sept. 2011; Phoenix. AZ. USA: IEEE; 2011. p. 2568–2575.

[63] Guo Y, Li S, Lee A T L, Tan S, Lee C K, Hui S Y R. Single-Stage AC/DC Single-Inductor Multiple-Output LED Drivers. *IEEE Transactions on Power Electronics*. 2016. 31 (8): 5837–5850. Doi: 10.1109/TPEL.2015.2496247.

[64] H. Chen, Y. Zhang and D. Ma, "A SIMO Parallel-String Driver IC for Dimmable LED Backlighting With Local Bus Voltage Optimization and Single Time-Shared Regulation Loop," in *IEEE Transactions on Power Electronics*, vol.

27, no. 1, pp. 452–462, Jan. 2012, doi:  
10.1109/TPEL.2011.2160404.

[65] Li S, Guo Y, Tan S, Hui S Y. An Off-line Single-Inductor Multiple-Output LED Driver with High Dimming Precision and Full Dimming Range. *IEEE Transactions on Power Electronics*. 2017; vol. 32; no. 6; p. 4716–4727. Doi: 10.1109/TPEL.2016.2597237.

[66] Yi KH. High Voltage, Low Current High-Power Multichannel LEDs LLC Driver by Stacking Single-Ended Rectifiers with Balancing Capacitors. *Electronics*. 2020; 9(3):529. <https://doi.org/10.3390/electronics9030529>.

IntechOpen